UiO : Department of Geosciences
University of Oslo

Idealized models of Polar Amplification

Jan-Adrian H. Kallmyr

Master's Thesis, Autumn 2021

Abstract

To study polar amplification (PA), two idealized energy balance models are constructed: a dry-diffusive down-gradient model (diffusion model) and a model where horizontal heat fluxes are configured in such a way as to maximize entropy production (MEP model). The effect of spherical geometry and non-uniform tropopause height is investigated in both models by comparing with a "cartesian model" with flat tropopause in both frameworks, and the baseline temperature anomaly from a decrease in planetary emissivity exhibits tropical amplification (TA). For the diffusion model, spherical geometry has minimal effect on the temperature anomaly, even though the resulting differences in volume is large between the poles and tropics. Similarly, having a non-uniform tropopause height has minimal effect on the temperature anomaly. A non-uniform diffusivity increases contrasts between polar and tropical regions, and may contribute either to PA or TA depending on which parameter is perturbed. All of these aforementioned contributions to the temperature profile are shown to be represented by "advection" velocities. In the MEP model, geometric considerations are shown to be irrelevant for the calculated heat transport.

PA is found to be affected by polar albedo decrease, which is well known, but also another hitherto unexplored mechanism, that of tropopause height increase (THI). Increasing the tropopause height uniformly yields a polar amplified temperature anomaly in all diffusion models. This effect is dependent on the magnitude of the diffusivity in the models. A comparison in Polar Amplification Factor (PAF) to albedo decrease is made for realistic values, and in the diffusivity range $10^6\,\mathrm{m^2 s^{-1}}$ – $10^7\,\mathrm{m^2 s^{-1}}$ THI yields comparable magnitudes. A study in asymmetries between the Arctic and Antarctica is also made, and it is found that while the elevation of the Antarctic continent ($H \approx 2500$m) should increase the warming effect of THI, the assumed lower diffusivities there restricts this heat transport. Finally, analytical results from the maximum entropy production (MEP) model suggests that the effect produced by THI may be counteracted. A suggested mechanism for this is that of simultaneous diffusivity decrease.

Acknowledgements

I would like to thank my supervisor Joe for inspiring me to pursue the following research, as well as accommodating my curiosity of extremum principles, dynamics and thermodynamics. While the Maximum Entropy Production principle turned out to be a lesser part of the thesis than was originally intended, the joy of surprises was ever present, and the experience of not being entirely certain where your research is headed is one I will keep with me in my future work as a sign of encouragement to explore more. Even though we end up repeating ourselves occasionally, the discussions about the thesis and science in general has always been very helpful, and I am grateful for always finding an open door.

I am very appreciative of the encouragement provided by meeting friends at the reading room every day, and the two years spent together have been wonderful! The uncertainty related to the pandemic has been much relieved due to the solidarity and camaraderie shown.

Conclusionary, I would like to thank Anna Lina for being there during my years spent at Blindern and elsewhere. Furthermore, I would like to thank my family for their presence, as well as my quark and rat friends for their splendid company.

To end is an excerpt from the beginning of "Vanitas, Vanitatum, Vanitas" by J. W. von Goethe:

> On nothing have I set my heart,
> Hurrah!
> So in the world I bear my part,
> Hurrah!

Jan-Adrian H. Kallmyr,

1st July 2021,

Oslo

Contents

List of Figures

List of Tables

List of Abbreviations

PA	polar amplification
TA	tropical amplification
ESM	earth system model
AA	arctic amplification
EBM	energy balance model
GCM	general circulation model
MEP	maximum entropy production
PAF	Polar Amplification Factor
THI	tropopause height increase
DD	diffusivity decrease
PDE	partial differential equation
ODE	ordinary differential equation
RHS	right-hand side
LHS	left-hand side
NH	northern hemisphere
SH	southern hemisphere
MHT	meridional heat transport
NCEP	National Centers for Environmental Prediction
GHG	greenhouse gas
TOA	top of the atmosphere

CHAPTER 1

Introduction

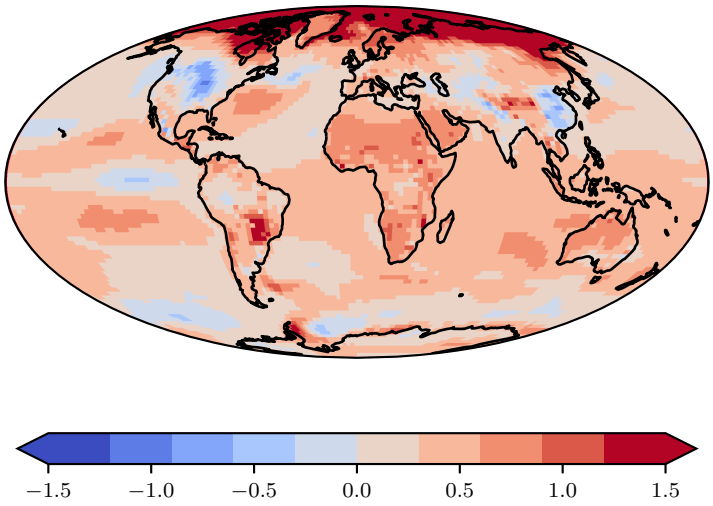

Figure 1.1: Historical near surface temperature anomaly in NorESM2-LM. Projection: Mollweide.

Global observations of surface temperature shows larger anomalies in the polar regions compared with lower latitudes. A phenomenon commonly called polar amplification (PA), PA is complex and exhibits regionaltiy as well as asymmetry between the south and north pole. Amplification in Antarctica is almost exclusively constrained to West Antarctica, and the Arctic is heating more than Antarctica; around twice as fast as lower latitudes (Bekryaev et al., 2010). While PA is present in earth system models (ESMs) (see Figure 1.1 for illustration), a complete understanding of the phenomenon is lacking. An area under active research (Smith et al., 2019), understanding polar amplification is important due to a myriad of factors. The enhanced warming in the arctic may indicate the extent and consequences of warming before a similar level of warming is achieved at lower latitudes. A rapidly changing polar climate may exhibit feedback behaviour in permafrost (Schaefer et al., 2014) and glacier melt which have global consequences (Overland et al., 2019). Understanding PA may yield insight into a general circulation perspective of the climate if e.g. oceanic and atmospheric heat transport are important contributors.

Different mechanisms for PA are proposed in the literature, such as the ice-albedo feedback (Screen and Simmonds, 2010), the lapse rate feedback (Stuecker et al., 2018), and general changes in the atmospheric (Armour et al., 2019) and oceanic heat transport (Mahlstein and Knutti, 2011; Marshall et al., 2015). The relative importance of these contributions are as of yet unknown, even though a recent study by Dai et al., 2019 suggests that sea ice melt is necessary for strong arctic amplification (AA). This would likewise explain the hemispheric asymmetry due to less sea ice cover and subsequently less sea ice melt in Antarctica, however, L. C. Hahn et al., 2020 argued that the lapse-rate feedback is the dominant driver of PA, and that the elevation of the Antarctic continent is what causes the asymmetry. The focus of this thesis, however, will be on possible large-scale contributors to PA, such as volume differences between lower and higher latitudes, changes in the tropopause height, and changes in the diffusivity.

One way to explore possible large-scale mechanisms of PA is to construct idealized models where we have control over model parameters and complexity. A simple model can provide conceptual understanding of the underlying processes that leads to PA. Budyko, 1969 introduced the concept of energy balance models (EBMs), which are simple models where only the zonal mean energy transfer between latitude bands is considered. The models are forced by incoming solar radiation, and often the earth is modeled as a gray-body. EBMs have been formally studied, and provides good representation of climate (North, 1975). These are ideal models for our study due to their simplicity and versatility in choice of model parameters. Recently, EBMs were used by Armour et al., 2019 to study the response of atmospheric meridional heat transport to greenhouse gas (GHG) forcing.

Another type of EBM is that of maximum entropy production (MEP) models, where the horizontal energy convergence is assumed to maximize entropy production. These models were pioneered by Paltridge, 1975 who developed a zonal mean climate model showing good agreement with observations. MEP models have also been developed and used recently, by e.g. Gjermundsen et al., 2014 who studied the shift of the mid-latitude storm tracks under GHG forcing.

Limiting the scope of the thesis, we will construct simple EBMs of the troposphere with no surface interactions to study PA, and compare the temperature and heat transport of these models with ESM NorESM2-LM. In particular, a central question is:

- how does the spherical geometry of the Earth and troposphere affect the profile of the global temperature anomaly under a global warming scenario?

With decreasing surface area and tropopause height polewards, the tropospheric volume decreases, which might influence the energy needed to heat the poles compared with lower latitudes.

Vallis et al., 2015 studied how the tropopause height changes under global warming. It is then natural to ask:

- does tropopause height increase (THI) contribute to PA?

- does the elevation of Antarctica and the larger THI-trend there (Vallis et al., 2015, Figure 7a) contribute to hemispherically asymmetric PA in an meridional heat transport (MHT) perspective?

Additionally,

- how does the atmospheric diffusivity look in NorESM2-LM?
- does it change under global warming and does this change contribute to PA?

These are the many questions to be addressed in this thesis.

The rest of the text is organized as follows:

Chapter 2 presents physical principles and a measure of PA used throughout the thesis, as well as details regarding the usage of NorESM2-LM.

Chapter 3 develops idealized EBM models using two different horizontal flux schemes, presents numerical methods for solving them, and investigates their limit behaviour.

Chapter 4 presents central results of the thesis, such as comparisons with NorESM2-LM, temperature anomalies under perturbation scenarios and the comparisons of the Polar Amplification Factor between perturbation scenarios.

Chapter 5 concludes the thesis by stating the main findings of the thesis, their possible consequences, before discussing possible future work.

Appendix A shows figures that may be of interest to some readers, and which are referred to but does not warrant their own presentation or discussion.

Appendix B features equations used in derivations for easy reference, as well as a segment of algebra omitted in the full text.

Appendix C consists of python classes developed to solve the two different model types.

CHAPTER 2

Theory and methods

To construct energy balance models there are ingredients which are needed, such as a vertical radiative flux model which simulates solar input and the radiation from Earth. This is what drives the model, but central to EBMs is horizontal heat transport which redistributes heat in the atmosphere. This section will derive a simple vertical radiation model and two different types of parameterizations of horizontal heat transport: a diffusion model and a MEP model. Additionally, a central measure of PA is presented. Finally, the data which was used from NorESM2-LM is presented in two tables alongside a description of how calculations were made.

For derivaties, the following notation is used for partial derivatives

$$\partial_{q_i} f(q_1, q_2, \dots) \equiv \frac{\partial}{\partial q_i} f(q_1, q_2, \dots).$$

In equilibrium, the partial differential equations (PDEs) reduces to ordinary differential equations (ODEs), and so technically the partial derivatives are transformed to ordinary derivatives. We will keep the same notation for these equations, but bear in mind that it represents slightly different concepts based on the context.

2.1 Simple gray-body radiation model

Common for all of the following models is a very simple model for the net solar radiative flux, which we will now construct.

Let us assume that the sun radiates as a black-body, while the atmosphere radiates as a grey-body with emissivity ϵ and absorptivity $\mu = 1 - \alpha$, where α is the albedo. The outgoing radiative flux is then, from the Stefan-Boltzmann law

$$F_\uparrow = \epsilon \sigma T^4, \tag{2.1}$$

where σ is the Stefan-Boltzmann constant, and T is the temperature of the atmosphere.

To find the incoming radiative flux we make a few geometric considerations (see Figure 2.1). The sun has a radius R_s and radiates in all directions in space

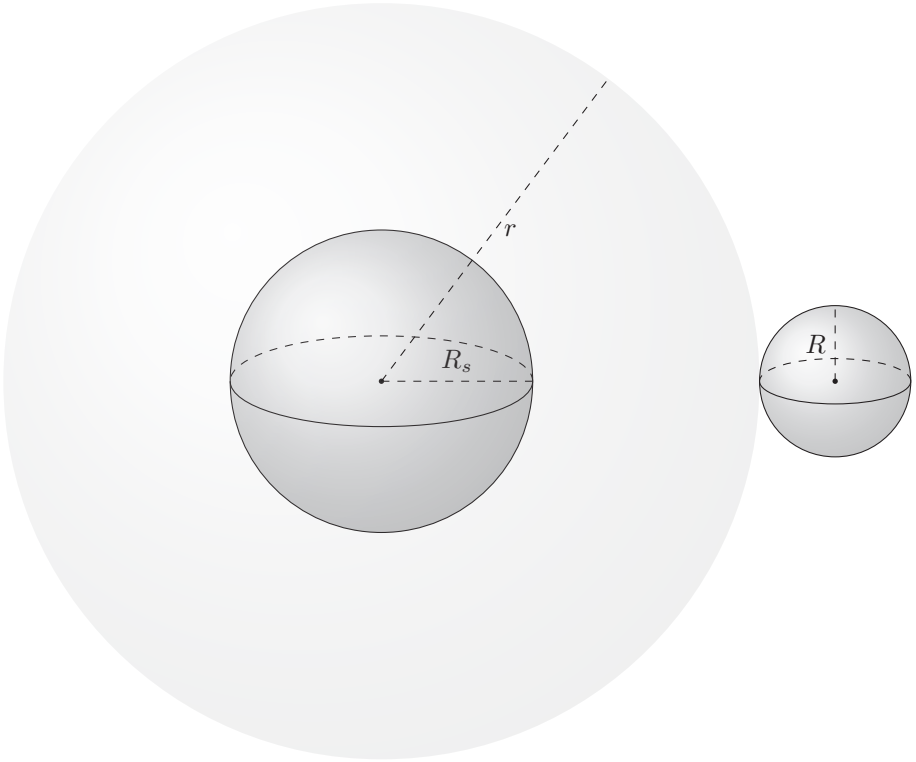

Figure 2.1: Sketch of the Sun-Earth system. The light-grey sphere illustrates radiation from the sun in all directions.

from its surface, and so using the Stefan-Boltzmann law again, the luminosity of the sun is

$$L_s = 4\pi R_s^2 \sigma T_s^4. \tag{2.2}$$

As the sun radiates, we can imagine a spherical shell with radius r which is how far the radiation has reached in all directions. Reaching the atmosphere, r is the distance between the atmosphere and the sun. The radiative flux that interacts with the atmosphere is then given by the sun's luminosity divided equally throughout the spherical shell

$$F_r = \frac{4\pi R_s^2 \sigma T_s^4}{4\pi r^2} = \frac{R_s^2}{r^2}\sigma T_s^4. \tag{2.3}$$

we assume that the Earth is far away, and small compared to the sun. Consequently, the total energy absorption from the incoming radiative flux is given by integrating over the area of Earth's shadow, i.e. a circle with the radius of the Earth with atmosphere R. The result is that the total energy absorbed by the atmosphere is

$$E = \mu F_r \sigma T_s^4 \pi R^2 = (1-\alpha)\frac{R_s^2}{r^2}\sigma T_s^4 \pi R^2. \tag{2.4}$$

In radiative balance, the incoming radiative flux must then be given by

$$F_\downarrow 4\pi R^2 = (1-\alpha)\frac{R_s^2}{r^2}\sigma T_s^4 \pi R^2 \quad \Leftrightarrow \quad F_\downarrow = s(1-\alpha), \tag{2.5}$$

where $s \equiv \sigma T_s^4 R_s^2 / 4r^2$ is the solar "constant", and is taken to be constant. Subtracting eq. 2.1 from eq. 2.5 we get the net solar radiative flux:

$$F_S = F_\downarrow - F_\uparrow = s(1-\alpha) - \epsilon\sigma T^4. \tag{2.6}$$

From eq. (2.6) we can find the equilibrium temperature T_e by assuming energy balance

$$T_e = \left(\frac{s(1-\alpha)}{\epsilon\sigma} \right)^{\frac{1}{4}}, \tag{2.7}$$

which tells us that a decrease of emissivity yields an increase in temperature.

2.2 The Law of Heat Conduction

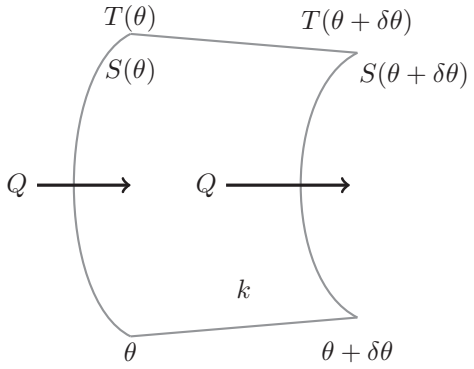

Figure 2.2: Schematic of heat conduction through a material.

Colloquially known as Fourier's law, the law of heat conduction states that the heat transfer is negatively proportional to the temperature gradient in a material. In integral form, the law takes the form

$$\partial_t Q = -k \oiint_S \boldsymbol{\nabla} T \cdot \mathrm{d}\mathbf{S}\,, \tag{2.8}$$

where k is the thermal conductivity, and $\mathrm{d}\mathbf{S}$ denotes an oriented surface element, which is chosen parallel to the heat transfer $\partial_t Q$. Figure 2.2 illustrates the different components of eq. (2.8). Fourier's law relates to gases from the relationship between thermal conductivity and thermal diffusivity:

$$D = \rho c_p k. \tag{2.9}$$

Here ρ is the density of the gas, and c_p is the specific heat under constant pressure.

Assuming no internal or external heat generation, the temporal change in heat is proportional to the temporal change in temperature

$$\partial_t Q = \rho c_p \iiint_V \partial_t T \,\mathrm{d}V\,. \tag{2.10}$$

Employing eqs. (2.9) and (2.10), eq. (2.8) becomes

$$\iiint_V \partial_t T \, \mathrm{d}V = -D \oiint_S \boldsymbol{\nabla} T \cdot \mathrm{d}\mathbf{S} \,. \tag{2.11}$$

In this form, Fourier's law relates the temporal change in temperature with the temperature distribution in the volume.

2.3 Diffusion Models

The annual and zonally averaged atmosphere can be conceptualised as a set of latitudinally constrained air masses which exchange heat with each other. Combined with some parameterisation of horizontal heat transfer, this framework allows for the construction of climate models without explicit dynamics. Such a EBM was first explored by Budyko, 1969 and have taken on many forms since then. The key advantage of EBMs are that they are simple compared with more advanced general circulation models (GCMs) or ESMs. This makes them suitable for a study on the effect of the geometry of the troposphere, as well as other model parameters.

Assuming the atmosphere obeys eq. (2.8) and radiates as a grey body (eq. (2.6)), the heat evolution of the system is

$$\partial_t Q = \iint_A \left[s(1-\alpha) - \epsilon\sigma T^4 \right] \mathrm{d}A - k \oiint_S \boldsymbol{\nabla} T \cdot \mathrm{d}\mathbf{S} \,, \tag{2.12}$$

where the first term on the right is integrated over the surface area $\mathrm{d}A$, and the second over the boundary between two latitudes $\mathrm{d}S$. While it makes no mathematical difference, the thermal diffusivity in a heat exchange model of the atmosphere is replaced with the eddy diffusivity, which has significantly greater magnitudes than e.g. the thermal diffusivity of air. In this conceptual framework, macroscopic atmospheric eddies are modeled akin to air molecules in a microscopic system.

2.4 Maximum Entropy Production models

The climate is a non-equilibrium non-linear thermodynamic system which is assumed to be in steady state. Such non-linear systems can evolve into an ensemble of different states depending on small perturbations in the initial conditions.

An hypothesis of a principle of MEP was first explored for the climate system by Paltridge, 1975 who argued that the climate state is that of a maximum in entropy production (Ozawa et al., 2003). Paltridge's model included the ocean which he assumed to act similarly to the atmosphere, as well as clouds and latent heat transport. The model compared favourably to observations of the meridional temperature distribution, heat transport, and cloud cover, however, the validity of such comparisons as confirmation of climate models has been questioned by e.g. Stone, 1978. Central to his model were two hypotheses (O'brien and Stephens, 1995):

1. Convection hypothesis - that the surface temperature and cloud fraction adjust in such a way as to maximize meridional heat fluxes
2. Maximum entropy production hypothesis - that the meridional energy convergence maximizes entropy production

While both of these assumptions were just as important (O'brien and Stephens, 1995), the maximum entropy production hypothesis as a physical principle gained the most traction. The MEP principle has also been explored observationally (Stephens and O'brien, 1993), but the principle remains an hypothesis. In this thesis, MEP is taken as a postulate and serves to include diffusion as an internal part of the model, rather than being prescribed as in a diffusion model.

Mathematically, the MEP principle can be stated as follows. The thermodynamic entropy of a system is

$$\mathrm{d}S = \frac{\Delta Q}{T}, \tag{2.13}$$

where ΔQ is the change in heat in the system, and T is the temperature of the system. MEP is the statement that

$$\partial_t S = \frac{\partial_t Q}{T} \tag{2.14}$$

is maximised.

2.5 Polar Amplification Factor

A useful measure of PA is the Polar Amplification Factor (PAF)

$$\mathrm{PAF} \equiv \frac{\Delta T_p}{\Delta \langle T \rangle}, \tag{2.15}$$

where ΔT_p denotes the temperature anomaly in a polar region (mean temperature polewards of 80°) and $\Delta \langle T \rangle$ denotes the globally averaged temperature anomaly.

If there is PA, then PAF > 1, while PAF < 1 implies tropical amplification (TA).

2.6 NorESM2-LM data and availability

For comparison we use data from a more complex ESM NorESM2-LM. Due to the simplicity of the models developed in this thesis, a rigourous comparison is not the aim, rather we would like to get a rough measure of how realistic the models are by comparing atmosphere-dominated measures. The CMIP6 experiments used are detailed in Table 2.1 while the variables are listed in Table 2.2.

The historical scenario and the near-surface temperature were used to create Figure 1.1. A climatology of pre-industrial and "present" values were calculated before calculating the anomaly. To obtain a meridional profile of the other

Table 2.1: Description of NorESM2-LM experiments used.

Experiments	**Description**
piControl	climate state without anthropogenic CO2 emissions
historical	climate state based on historical forcing

variables (or derived variables) in Table 2.2 a climatology is first calculated before taking the longitudinal average. Air temperature is also a function of pressure, and a mean atmospheric value is calculated by taking the density-weighted mean using standard functions from the *geonum.atmosphere*-package. The stratosphere is included in this calculation, however, the density-weighting ensures that its contribution is much less compared with the troposphere.

Table 2.2: Description of NorESM2-LM variables used from each experiment.

Variables	**Description**
ta	air temperature
tas	near-surface air temperature
rlut	outgoing longwave radiation
rsut	outgoing shortwave radiation
rsdt	incoming shortwave radiation

CHAPTER 3

Model development

Using the theoretical foundations established in the previous section, we will now construct the diffusion and MEP models, respectively. To begin, the geometry of the troposphere will be presented, before constructing a simple cartesian diffusion model to act as baseline for diffusion model experiments. The full generalized diffusion model will then be developed and an analysis of equilibrium perturbations conducted, before scaling the full equation and presenting a discretisation scheme. The MEP model is then developed using the method of Lagrange multipliers before we include a summary of parameters used in the models.

3.1 Geometry of the troposphere

We will construct various EBMs throughout the thesis which all have the same set-up. Figure 3.1a shows a schematical representation of a latitude band from latitude θ to latitude $\theta + \delta\theta$ as seen from space. $A(\theta)$ is the surface area of a sphere and L is the cicle of latitude. The geometry in the vertical can be seen in Figure 3.1b, where H is the tropopause height. Central to our calculations will turn out to be the surface area A and the cross-sectional area $S \equiv LH$ at each latitude. Referred to henceforth as boxes, these latitude bands represent zonal mean parameters and variables of the model.

Each box is connected to another through incoming and outgoing heat fluxes, as shown in Figure 3.2. The vertical fluxes are common for all models, and are illustrated in Figure 3.3. Additionally, the cartesian boxes are easily obtained from the more general boxes, and so are not illustrated here.

3.2 Simple cartesian model

To act as a baseline a simple cartesian model will be developed. Assuming cartesian coordinates (x, y, z) and

$$\begin{aligned} A(y) &= \text{const.} \\ L(y) &= \text{const.} \\ H(y) &= \text{const.} \\ D(y) &= \text{const.}, \end{aligned}$$

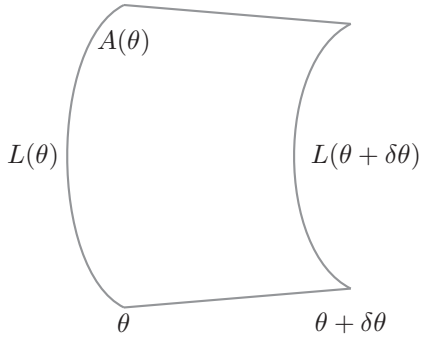

(a) Sketch of a area element of the surface of a sphere. Here A denotes the surface area and L the circumference of the latitude band.

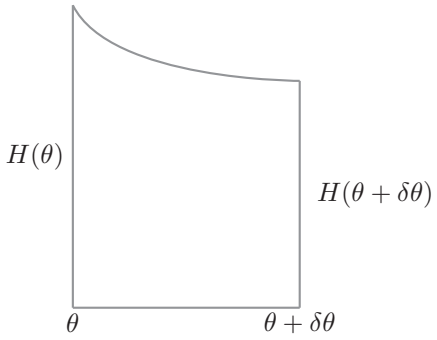

(b) Sketch of a vertical slice of the troposphere on a sphere. Here H denotes the tropopause height.

Figure 3.1: Geometrical set-up of the box models. Here θ denotes latitude.

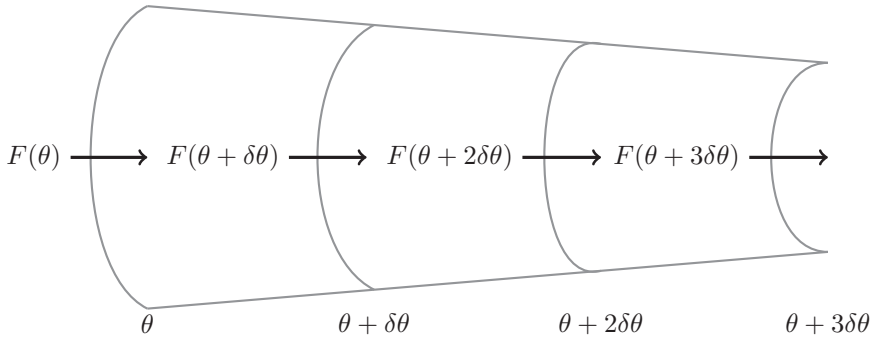

Figure 3.2: Schematic of lateral heat flux interactions between latitude bands from θ to $\theta + 3\delta\theta$.

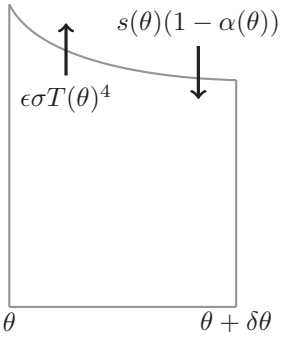

Figure 3.3: Schematic of vertical heat fluxes on a latitude band.

as well as a single (mean) temperature in the volume, then Fourier's law with external heating yields (eqs. (2.8) and (2.6))

$$L\delta y H \rho c_p \partial_t Q = L\delta y F_s - kLH\partial_y T(y) + kLH\partial_y T(y+\delta y). \tag{3.1}$$

Factoring and employing eqs. (2.9) and (2.10) reduces the equation to

$$\partial_t T = \tilde{F}_s - \frac{1}{\delta y} D\partial_y T(y) + \frac{1}{\delta y} D\partial_y T(y+\delta y), \tag{3.2}$$

where $\tilde{F}_s \equiv F_s/\rho c_p H$. Taylor-expanding the last term, the equation becomes

$$\partial_t T = \tilde{F}_s - \frac{1}{\delta y} D\partial_y T(y) + \frac{1}{\delta y}\Big[D\partial_y T + \partial_y(D\partial_y T)\delta y + \mathcal{O}\Big((\delta y)^2\Big)\Big]. \tag{3.3}$$

Canceling terms and neglecting $\mathcal{O}(\delta y)$-terms gives

$$\partial_t T = D\partial_y^2 T + \tilde{F}_s, \tag{3.4}$$

which is the inhomogeneous heat equation with constant diffusivity, D.

3.3 Generalized spherical model

Generalizing from the previous model, we will now take into account the geometry of the troposphere, as well as a non-uniform diffusivity profile.

A spherical coordinate frame centered at the equator is chosen yielding coordinates (r, θ, ϕ). Assuming the tropopause height H and diffusivity D are non-uniform, Fourier's law with external heating gives

$$\begin{aligned}\partial_t T = \tilde{F}_s &- \frac{L(\theta)H(\theta)}{A(\theta)H(\theta)R} D(\theta)\partial_\theta T \\ &+ \frac{L(\theta+\delta\theta)H(\theta+\delta\theta)}{A(\theta)H(\theta)R} D(\theta+\delta\theta)\partial_\theta T(\theta+\delta\theta).\end{aligned}$$

This expression can be simplified by canceling and Taylor-expanding while neglecting all $\mathcal{O}(\delta\theta)$-terms (after division). Dropping explicit θ-dependence, this is written out as

$$\begin{aligned}\partial_t T = \tilde{F}_s &- \frac{L}{A}\frac{D}{R}\partial_\theta T \\ &+ \frac{1}{AHR}[(L+\partial_\theta L\delta\theta)(H+\partial_\theta H\delta\theta)](D+\partial_\theta D\delta\theta)\big(\partial_\theta T + \partial_\theta^2 T\delta\theta\big).\end{aligned}$$

This reduces to

$$\begin{aligned}\partial_t T = \tilde{F}_s &- \frac{L}{A}\frac{D}{R}\partial_\theta T \\ &+ \frac{1}{AHR}\big[LHD\partial_\theta T + \delta\theta(LH\partial_\theta D + LD\partial_\theta H\delta\theta + DH\partial_\theta L)\partial_\theta T + LHD\partial_\theta^2 T\delta\theta\big],\end{aligned}$$

where the second term cancels, yielding

$$\partial_t T = \tilde{F}_s + \delta\theta\left[\left(\frac{L}{AR}\partial_\theta D + \frac{LD}{ARH}\partial_\theta H + \frac{D}{AR}\partial_\theta L\right)\partial_\theta T + \frac{LD}{AR}\partial_\theta^2 T\right].$$

A common factor can be extracted as follows

$$\partial_t T = \tilde{F}_s + \delta\theta \frac{LD}{AR}\big[(\partial_\theta \ln D + \partial_\theta \ln H + \partial_\theta \ln L)\partial_\theta T + \partial_\theta^2 T\big]. \tag{3.5}$$

Now it is beneficial to calculate the surface area A and the zonal circumference L. With Jacobian-determinant $J(r, \theta, \phi) = R^2 \cos\theta$, the surface area is

$$\begin{aligned} A &= \int_0^{2\pi} \int_\theta^{\theta+\delta\theta} R^2 \cos\theta' \, \mathrm{d}\theta' \, \mathrm{d}\phi' \\ &= 2\pi R^2 [\sin(\theta + \delta\theta) - \sin\theta]. \end{aligned}$$

Using the trigonometric addition rule for sines (eq. (B.2))

$$A = 2\pi R^2 [\sin\theta \cos\delta\theta + \cos\theta \sin\delta\theta - \sin\theta]. \tag{3.6}$$

This expression is simplified by assuming the angle $\delta\theta$ is small, which is consistent with only keeping $\mathcal{O}(\delta\theta)$-terms previously. Using the trigonometric identities eqs. B.3 and B.4 then gives a relatively simple expression for A

$$A = 2\pi R^2 [\cos\theta\delta\theta + \sin\theta - \sin\theta] = 2\pi R^2 \delta\theta \cos\theta. \tag{3.7}$$

L is similarly calculated as

$$L = \int_0^{2\pi} R\cos\theta \, \mathrm{d}\phi = 2\pi R \cos\theta,$$

and the gradient is

$$\partial_\theta L = -2\pi R \sin\theta. \tag{3.8}$$

Inserting expressions for A and L and its gradient into eq. (3.5) yields

$$\partial_t T = \tilde{F}_s + \gamma \partial_\theta^2 T + \gamma(\partial_\theta \ln D + \partial_\theta \ln H - \tan\theta)\partial_\theta T, \tag{3.9}$$

where $\gamma \equiv D/R^2$. The tangent term is a purely geometrical term, and the above expression can be rewritten more suggestively

$$\partial_t T = \tilde{F}_s + \gamma \sec\theta \partial_\theta(\cos\theta \partial_\theta T) + \gamma(\partial_\theta \ln D + \partial_\theta \ln H)\partial_\theta T. \tag{3.10}$$

Here the second term is the latitudinal component of the Laplacian in spherical coordinates, and affirms the method used. Additionally, we can define an "advection" velocity

$$v(\theta) \equiv R\gamma(\tan\theta - \partial_\theta \ln D - \partial_\theta \ln H), \tag{3.11}$$

which serves to "advect" temperature, and is due to the variation in circle of latitude, tropopause height, and diffusivity. This has not previously been pointed out. Eq. (3.9) can then be rewritten in terms of the material derivative

$$(\partial_t + \frac{v}{R}\partial_\theta)T = \gamma \partial_\theta^2 T + \tilde{F}_s. \tag{3.12}$$

For practical purposes eq. (3.9) is used due to its transparent form and ease of discretization.

Discretisation

As the diffusion model is run forward in time to achieve equilibrium it is useful to normalize eq. (3.12) to find characteristic time scales. Since the time and spatial terms share a scale proportional to $1/t$ we get the relation

$$\frac{T}{t} \propto \frac{DT}{R^2} \quad \frac{\epsilon\sigma T^4}{\rho c_p H}. \tag{3.13}$$

Eq. (3.13) yields two time scales

$$t_{\text{diff}} \propto \frac{R^2}{D} = \frac{\left(6371 \cdot 10^3\right)^2}{5 \cdot 10^6}\,\text{s} \approx 94\,\text{days} \tag{3.14}$$

$$t_{\text{rad}} \propto \frac{\rho c_p H}{\epsilon\sigma T^3} = \frac{1(1004)(12.5 \cdot 10^3)}{0.8(5.67 \cdot 10^{-8})290^3}\,\text{s} \approx 131\,\text{days}, \tag{3.15}$$

a diffusive and radiative time scale, respectively. With this diffusivity (see eq. (3.60)), which was chosen to achieve a realistic temperature profile, diffusion acts significantly faster than radiative effects, and so the radiative time scale will be used to ensure that the model has reached equilibrium. We discretise eq. (3.9) using the Forward-Time-Centered-Space (FTCS) scheme, which is sufficient in this case, as investigated by LaCasce, 2020. This gives

$$T_j^{n+1} = T_j^n + \tilde{F}_{s,j}^n \Delta t + \frac{D_j}{R^2}\frac{\Delta t}{(\Delta\theta)^2}\left(T_{j+1}^n - 2T_j^n + T_{j-1}^n\right) + \frac{v_j \Delta t}{R\Delta\theta}\left(T_{j+1}^n - T_{j-1}^n\right), \tag{3.16}$$

where n and j are time and space indices, respectively. we can rewrite this in terms of the (spatially-variant) Courant number $C_0 \equiv v_j \Delta t (R\Delta\theta)^{-1}$ and stability parameter $s \equiv D_j \Delta t (R\Delta\theta)^{-2}$

$$T_j^{n+1} = \left(s_j - \frac{C_j}{2}\right)T_{j+1}^n + (1 - 2s_j)T_j^n + \left(s_j + \frac{C_j}{2}\right)T_{j-1}^n + \tilde{F}_{s,j}^n \Delta t. \tag{3.17}$$

As diffusion acts to redistribute heat but is otherwise conservative, a reasonable choice of boundary conditions are the Neumann boundary conditions, i.e. zero lateral temperature flux at the poles:

$$T_{-1}^n = T_1^n \qquad T_{J+1}^n = T_{J-1}^n, \tag{3.18}$$

where T_{-1}^n and T_{J+1}^n are the temperatures at the boundaries. Inserting this into the equations at the boundaries, we can rewrite eq. (3.17) as a matrix equation

$$\mathbf{T^{n+1}} = A\mathbf{T^n} + \mathbf{F_s^n} \tag{3.19}$$

where

$$A \equiv \begin{bmatrix} 1-2s & 2s & 0 & \dots & \dots & 0 \\ s + \frac{C_0}{2} & 1-2s & s - \frac{C_0}{2} & 0 & \dots & 0 \\ 0 & s + \frac{C_0}{2} & 1-2s & s - \frac{C_0}{2} & \dots & 0 \\ \vdots & \ddots & \ddots & \ddots & \ddots & \vdots \\ 0 & \dots & \ddots & s + \frac{C_0}{2} & 1-2s & s - \frac{C_0}{2} \\ 0 & \dots & \dots & 0 & 2s & 1-2s \end{bmatrix}, \tag{3.20}$$

and

$$\mathbf{T^n} \equiv \begin{bmatrix} T_0^n \\ T_1^n \\ \vdots \\ T_J^n \end{bmatrix} \qquad \mathbf{F_s^n} \equiv \begin{bmatrix} \tilde{F}_{s,0}^n \\ \tilde{F}_{s,1}^n \\ \vdots \\ \tilde{F}_{s,J}^n \end{bmatrix} \Delta t, \tag{3.21}$$

The matrix product is inefficient to calculate as A is tridiagonal, however, due to the addition of $\mathbf{F_s^n}$ we cannot solve it using a Gaussian elimination algorithm. Another approach is to store the left, main, and right diagonals as vectors $\mathbf{C_0}$, $\mathbf{C_1}$, $\mathbf{C_2}$ respectively, and write eq. (3.19) in terms of shifted temperature vectors

$$\mathbf{T}^{n+1} = \mathbf{C_0} \circ \tilde{\mathbf{T}}_\mathbf{1}^\mathbf{n} + \mathbf{C_1} \circ \mathbf{T^n} + \mathbf{C_2} \circ \tilde{\mathbf{T}}_\mathbf{2}^\mathbf{n} + \mathbf{F_s^n}, \tag{3.22}$$

where $\circ$ is the elementwise multiplication operator, and the shifted temperature vectors are defined as follows:

$$\tilde{\mathbf{T}}_\mathbf{1}^\mathbf{n} \equiv \begin{bmatrix} 0 \\ T_0^n \\ T_1^n \\ \vdots \\ T_{J-1}^n \end{bmatrix} \qquad \tilde{\mathbf{T}}_\mathbf{2}^\mathbf{n} \equiv \begin{bmatrix} T_1^n \\ T_2^n \\ \vdots \\ T_J^n \\ 0 \end{bmatrix}. \tag{3.23}$$

Note that the zero in each vector is to make the vectors equal length and satisfy boundary conditions.

Equilibrium perturbations

To investigate qualitatively how the system might change under global warming we will look at the steady-state of eq. (3.9) and perturb it in parameters that are expected to change due to GHG emissions.

Assuming spherical geometry, varying tropopause height, and varying diffusivity the equilibrium equation of the system becomes

$$s(1-\alpha) - \epsilon\sigma T^4 + \Gamma H \partial_\theta^2 T + (H\partial_\theta \Gamma + \Gamma \partial_\theta H - \Gamma H \tan\theta)\partial_\theta T = 0 \tag{3.24}$$

where $\Gamma \equiv \rho c_p \gamma$. The equation can be further simplified as

$$s(1-\alpha) - \epsilon\sigma T^4 + \Gamma H \partial_\theta^2 T + (\partial_\theta(\Gamma H) - \Gamma H \tan\theta)\partial_\theta T = 0. \tag{3.25}$$

Defining a diffusion operator

$$\tilde{\nabla}^2(AB) \equiv \sec\theta \partial_\theta(\Gamma A \cos\theta \partial_\theta B), \tag{3.26}$$

Eq. (3.25) can be re-written

$$s(1-\alpha) - \epsilon\sigma T^4 + \nabla^2(HT) = 0 \tag{3.27}$$

Accounting for possible perturbations due to a GHG emissions (which we represent by a emissivity perturbation), we let $\epsilon \to \epsilon + \Delta\epsilon$, $T \to T + \Delta T$, $\alpha \to \alpha + \Delta\alpha$, $H \to H + \Delta H$. Perturbing eq. (3.27) and assuming changes are small (so that the base state is still satisfied) the equation becomes

$$\tilde{\nabla}^2(H\Delta T) - 4\epsilon\sigma T^3 \Delta T = s\Delta\alpha + \Delta\epsilon\sigma T^4 - \tilde{\nabla}^2(\Delta H T), \tag{3.28}$$

which is a ODE for ΔT with forcing terms on the right-hand side (RHS).

Extreme diffusion limits

Letting $\gamma = 0$ (hence $\Gamma = 0$), so that the diffusion-terms vanish, eq. (3.28) yields the following expression for the temperature anomaly

$$\Delta T = -\frac{s\Delta\alpha}{4\epsilon\sigma T^3} - \frac{\Delta\epsilon}{4\epsilon}T. \tag{3.29}$$

Assuming there is no change in albedo, $\Delta\alpha = 0$, and a negative emissivity change, $\Delta\epsilon < 0$, then $\Delta T \propto T$. The temperature anomaly mirrors the base state temperature, which we know is tropically amplified, and so the response is also tropically amplified.

A negative change in albedo $\Delta\alpha < 0$ and no emissivity change $\Delta\epsilon = 0$ leaves the first term on the right where s favours TA, but T^{-3} favours PA. Which term will dominate is non-trivial, and will be explored numerically. Additionally, a local negative albedo change, such as is the case with sea-ice melt, will amplify the warming there.

Conversely, in the limit where $\gamma \to \infty$ ($\Gamma \to \infty$), eq. (3.28) reduces to

$$\tilde{\nabla}^2(H\Delta T) = 0 \Rightarrow \Delta T = \text{const.}, \tag{3.30}$$

which yields globally uniform warming, which is common for all diffusive systems in this limit, as the gradients driving transport vanish.

Intermediate diffusion limit

In this case the analysis is restricted by assuming a constant tropopause height and change in tropopause height. The last term on the right in eq. (3.28) can then be written in terms of the base state diffusion term (see eq. (3.27))

$$-\tilde{\nabla}^2(\Delta HT) = -\frac{\Delta H}{H}\tilde{\nabla}^2(HT) = \frac{\Delta H}{H}\big[s(1-\alpha) - \epsilon\sigma T^4\big]. \tag{3.31}$$

To get at a qualitative temperature anomaly under intermediate diffusion we will neglect the first term on the left-hand side (LHS) in eq. (3.28), and thereby focus on the RHS, which yields an approximation for the temperature anomaly

$$\Delta T \approx -\frac{s\Delta\alpha}{4\epsilon\sigma T^3} - \frac{\Delta\epsilon}{4\epsilon}T - \frac{\Delta H}{4\epsilon\sigma T^3 H}\big[s(1-\alpha) - \epsilon\sigma T^4\big], \tag{3.32}$$

where the two first terms are known from the no diffusion limit and the last term is an addition from tropopause height perturbation. As can be seen from eq. (3.32), THI $\Delta H > 0$ will tend to favour polar enhancement due to its dependency on the net radiation balance which has a deficit in the polar regions and T^{-3}. This term also exhibits tropical cooling due to the surplus in the net radiation balance there, and is the only term to do so. THI acts to redistribute heat from the base state, cooling the equator and warming the poles. Not discussed elsewhere, this term is a potential contributor to PA.

3.4 Perturbed two box model

As simplicity is also a goal of this thesis, we will demonstrate how the previous perturbation behaviour is all present in a simple 2-box model. The reader may skip ahead to Section 3.5 if they are eager to be introduced to the MEP model.

Assuming that we can divide the atmosphere into two volumes: lower and higher latitudes. In equilibrium, the equations describing the heat transfer from lower to higher latitudes are

$$s_1(1-\alpha_1) - \epsilon\sigma T_1^4 + \rho c_p \frac{DH}{A_1 R^2}(T_2 - T_1) = 0 \tag{3.33}$$

$$s_2(1-\alpha_2) - \epsilon\sigma T_2^4 - \rho c_p \frac{DH}{A_2 R^2}(T_2 - T_1) = 0, \tag{3.34}$$

where $s_1 > s_2$ and $T_1 > T_2$. Defining a parameter $\zeta \equiv \Gamma A_1^{-1} = \rho c_p D R^{-2} A_1^{-1}$, and the area-ratio $n \equiv A_1/A_2$, the equations can be re-written

$$s_1(1-\alpha_1) - \epsilon\sigma T_1^4 + \zeta H(T_2 - T_1) = 0, \tag{3.35}$$

$$s_2(1-\alpha_2) - \epsilon\sigma T_2^4 - n\zeta H(T_2 - T_1) = 0. \tag{3.36}$$

Using the following perturbations

$$\begin{aligned} \epsilon &\to \epsilon + \Delta\epsilon \\ T_i &\to T_i + \Delta T_i \\ \alpha_i &\to \alpha_i + \Delta\alpha_i \\ H &\to H + \Delta H, \end{aligned}$$

and assuming they are relatively small,

$$\begin{aligned} \Delta\epsilon &<< +\epsilon \\ \Delta T_i &<< T_i \\ \Delta\alpha_i &<< \alpha_i \\ \Delta H &<< H, \end{aligned}$$

the equations become

$$-\big(4\epsilon\sigma T_1^3 + \zeta H\big)\Delta T_1 + \zeta H \Delta T_2 = s_1\Delta\alpha_1 + \Delta\epsilon\sigma T_1^4 - \zeta\Delta H(T_2 - T_1) \tag{3.37}$$

$$n\zeta H\Delta T_1 - \big(4\epsilon\sigma T_2^3 + n\zeta H\big)\Delta T_2 = s_2\Delta\alpha_2 + \Delta\epsilon T_2^4 + n\zeta\Delta H(T_2 - T_1). \tag{3.38}$$

This set of equations can be solved using Cramer's rule (eq. (B.6)) and the solutions share a common denominator

$$\begin{aligned} f &= \big(4\epsilon\sigma T_1^3 + \zeta H\big)\big(4\epsilon\sigma T_2^3 + n\zeta H\big) - n\zeta^2 H^2 \\ &= 16\epsilon^2\sigma^2 T_1^3 T_2^3 + 4\epsilon\sigma\zeta H\big(nT_1^3 + T_2^3\big) + n\zeta^2 H^2 - n\zeta^2 H^2 \\ &= 4\epsilon\sigma\big[4\epsilon\sigma T_1^3 T_2^3 + \zeta H\big(nT_1^3 + T_2^3\big)\big], \end{aligned} \tag{3.39}$$

which is positive, i.e. $f > 0$. The solutions can then be written out as

$$\begin{aligned} f\Delta T_1 = &-\big(4\epsilon\sigma T_2^3 + n\zeta H\big)\big[s_1\Delta\alpha_1 + \Delta\epsilon T_1^4 - \zeta\Delta H(T_2 - T_1)\big] \\ &- \zeta H\big[s_2\Delta\alpha_2 + \Delta\epsilon T_2^4 + n\zeta\Delta H(T_2 - T_1)\big] \end{aligned} \tag{3.40}$$

$$f\Delta T_2 = -\left(4\epsilon\sigma T_1^3 + \zeta H\right)\left[s_2\Delta\alpha_2 + \Delta\epsilon T_2^4 + n\zeta\Delta H(T_2 - T_1)\right] - n\zeta H\left[s_1\Delta\alpha_1 + \Delta\epsilon T_1^4 - \zeta\Delta H(T_2 - T_1)\right]. \tag{3.41}$$

The difference between the temperature anomalies is then (see eq. (B.7) for explicit calculation)

$$\begin{aligned} g(\Delta T_2 - \Delta T_1) =& \left(T_2^3 s_1\Delta\alpha_1 - T_1^3 s_2\Delta\alpha_2\right) \\ &+ \sigma\Delta\epsilon T_1^3 T_2^3(T_1 - T_2) \\ &+ \zeta\Delta H(T_1 - T_2)\left(nT_1^3 + T_2^3\right), \end{aligned} \tag{3.42}$$

where $g \equiv f/4\epsilon\sigma$.

Looking at the effect of each term in eq. (3.42) in isolation we see that there are local effects from albedo changes. A decrease in albedo in the tropics will heat up the tropics, and a decrease in albedo at the pole will heat up the pole. However, a decrease in emissivity $\Delta\epsilon < 0$ will cause tropical enhancement, while an increase in tropopause height $\Delta H > 0$ will cause polar enhancement.

Even in such an idealized 2-box model, much of the same structure can be found as in the continuous case. Eq. (3.42) also implies that PA due to THI is present even for cartesian geometry as then $n = 1$. Moreover, the n-dependency, which is the effect of non-equal volumes, implies that depending on where the boxes are defined the effect could be larger. Looking at the area ratio in Figure 3.4, we see that $n > 1$ after around 20°.

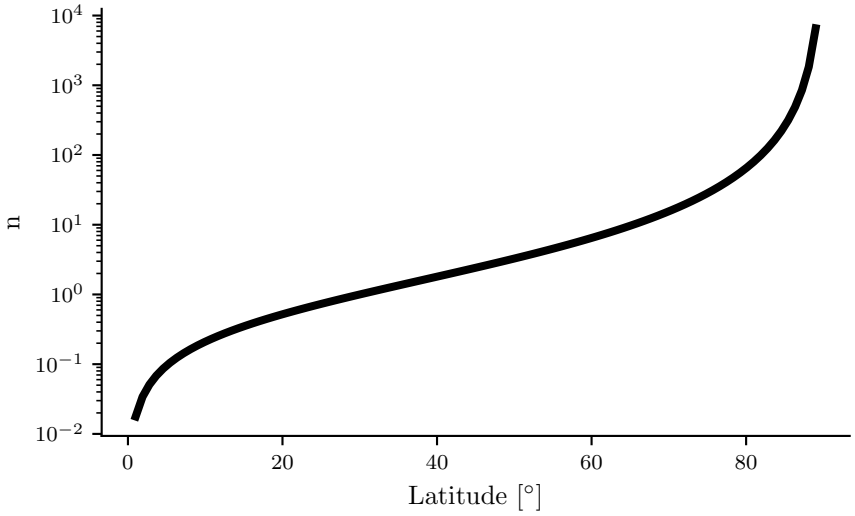

Figure 3.4: Area ratio of a sphere $n = \sin\theta/(1 - \sin\theta)$, logarithmic y-scale.

3.5 Maximum Entropy Production model

We will construct a similar model as done by Gjermundsen et al., 2014, which was a surface-atmosphere model where the horizontal and vertical heat transports

were parameterized by assuming the principle of MEP. Our model will be simplified and not include surface processes, so as to make it comparable to the diffusion model.

In our case, the energy balance equation in equilibrium for each box takes the form

$$F_{s,j}A_j + \Delta\partial_t Q_j = 0, \tag{3.43}$$

where $F_{s,j}$ is the net vertical radiation in each box, and

$$\Delta\partial_t Q_j \equiv F_j S_j - F_{j+1} S_{j+1} \tag{3.44}$$

is the meridional heat transfer. F_j and F_{j+1} are incoming and outgoing horizontal heat fluxes, respectively. The cross-sectional area S is defined in Figure 3.2. From eq. (3.43) we find the relation

$$\Delta\partial_t Q_j = -F_{s,j}A_j. \tag{3.45}$$

The meridional heat transfer only serve to redistribute heat, and so summing over all boxes they should sum to zero. This gives us the energy conservation constraint

$$g(\Delta\partial_t Q) \equiv \sum_{j=0}^{J} \Delta\partial_t Q_j = -\sum_{j=0}^{J} F_{s,j}A_j = 0. \tag{3.46}$$

To maximise eq. (2.14) we use the method of Lagrange multipliers (Lindstrøm and Hveberg, 2015, p. 528) to enforce energy conservation. This yields the Lagrangian in each box

$$L_j = \frac{1}{T_j}\Delta\partial_t Q_j + \beta g(\Delta\partial_t Q_j), \tag{3.47}$$

where β is a Lagrange multiplier.

The Lagrangian for the entire system is then just a sum over the entropy production and constraint in each box

$$L = \sum_{j=0}^{J} \left(\frac{\Delta\partial_t Q_j}{T_j} - \beta F_{s,j}A_j \right). \tag{3.48}$$

Inserting eq. (3.45) into eq. (3.48) we get

$$L = \sum_{j=0}^{J} \left(-\frac{F_{s,j}}{T_j} - \beta F_{s,j} \right) A_j. \tag{3.49}$$

Maximising the Lagrangian with regards to the temperature in each box we get the PDE

$$-T_j \frac{\partial F_{s,j}}{\partial T_j}(1 + \beta T_j) + F_{s,j} = 0. \tag{3.50}$$

Note that the geometrical contribution drops out of the equation. This is in contrast to the diffusion model where the geometry clearly affects the temperature distribution. Additionally, this means that the tropopause height has no effect on the temperature distribution in the MEP model.

Inserting for $F_{s,j}$ gives an algebraic equation

$$T_j^4(3 + 4\beta T_j) + \frac{s_j(1 - \alpha_j)}{\epsilon\sigma} = 0, \tag{3.51}$$

Looking at eq. (3.51) we see that a $\beta > 0$ yields no solutions since $T_j > 0$ and the constant term is positive and non-zero (see Figure 3.5a), and so β must be negative for there to be solutions. Letting $C_j \equiv s_j(1 - \alpha_j)/\epsilon\sigma$ we can rewrite eq. (3.51) as

$$T_j^4(3 + 4\beta T_j) = -C_j. \tag{3.52}$$

This equation can only have real solutions if $T_j > -3/4\beta$. Differentiating it yields

$$2T_j^3(6 + 10\beta T_j) = 0, \tag{3.53}$$

which is always negative and so by Rolle's theorem there can only be one real root.

This means that it's trivial to solve eq. (3.51) using Newton's method (Lindstrøm and Hveberg, 2015, p. 462). A reasonable guess for the temperature in each box is then

$$T_{j,guess} = -\frac{3}{4\beta}. \tag{3.54}$$

To find the maximum of the Lagrangian in eq. (3.48) we tune β so as to satisfy the constraint in eq. (3.46). In practice we use Newton's method twice: first for finding all the temperatures in each box, second for finding the beta that minimises eq. (3.46), ensuring energy conservation.

3.6 Parameters and velocities

While eq. (2.6) holds for a single-box atmosphere, the sun-atmosphere distance, and therefore the solar constant, will vary latitudinally. To account for this we parameterize the solar constant based on the climatology of the absorbed shortwave radiation from Hartmann, 2015, FIGURE 2.12.

$$s(\theta) = 325\cos\theta + 50. \tag{3.55}$$

The planetary albedo and emissivity are also non-trivial functions of latitude and have to be parameterised. From Donohoe and Battisti, 2011, Fig. 3a we parameterised the albedo

$$\alpha(\theta) = 0.7 - 0.45\cos\theta. \tag{3.56}$$

For simplicity, the baseline planetary emissivity is taken to be constant for the entire globe at a value

$$\epsilon = 0.80. \tag{3.57}$$

To simulate global warming, we will change the emissivity as a proxy for GHG emissions.

The tropopause is not at a constant height at all latitudes, rather, it decreases polewards. The height of the tropopause will be prescribed, and so we will

use a parameterization as for the solar constant and albedo. Based on NCEP2 reanalysis data (Vallis et al., 2015, FIGURE 1a) the shape of the tropopause is similar to a function $\cos 2\theta$. We will therefore use the parameterization

$$H(\theta) = (H_{max} - \langle H \rangle) \cos 2\theta + \langle H \rangle = \Delta H \cos 2\theta + \langle H \rangle \,, \tag{3.58}$$

where H_{max} is the maximum height of the tropopause located in equatorial regions, and $\langle H \rangle$ is the mean height of the tropopause. In constant tropopause height runs a value

$$H_{\text{const.}} = 12.5\,\text{km} \tag{3.59}$$

will be used.

The diffusivity profile was found by roughly tuning the model for NorESM2-LM air temperature output. Additionally, a physical argument is made as to the shape of the profile. From Hartmann, 2015, FIGURE 6.18 there should be a storm track (zonally averaged) in each hemisphere at mid-latitudes. The seasonal variation, however, suggests that there is a cyclical weakening of the storm tracks. Due to seasonal anti-symmetry between hemispheres we therefore assume that the annually mean, zonally averaged storm track is roughly centered at the equator. As the storm tracks are localized over a relatively small range of latitudes, we use a parameterization

$$D(\theta) \equiv \left(5 \cdot 10^6\right) \cos^{1.5}(\theta)\,\text{m}^2\text{s}^{-1}, \tag{3.60}$$

which yields a profile similar to that used in earlier papers (Sellers, 1969, TABLE 2). In constant diffusivity runs, the value

$$D_{\text{const.}} = 2.5 \cdot 10^6\,\text{m}^2\text{s}^{-1} \tag{3.61}$$

is used, which is roughly the average of the above profile.

All of the parameters used in the models are shown in Figure 3.5 for reference.

The "advection" velocities for the diffusion models are shown in Figure 3.6. For all cases, the velocity is poleward. In the constant diffusivity cases with constant tropopause height (dotted) and non-uniform tropopause height (dashed) we see two peaks at the poles. The tangent term seems to dominate as comparing the two as there is almost no difference. When including a non-uniform diffusivity profile (solid), the velocity changes having two small peaks at mid-latitudes and vanishing at the poles.

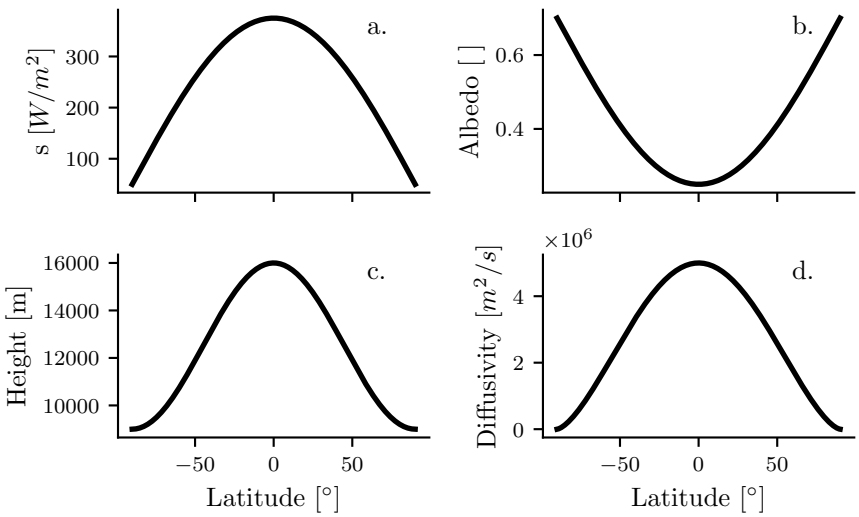

Figure 3.5: Shape of parameters used in the models: a. absorbed solar heat flux, b. planetary albedo, c. tropopause height, and d. Diffusivity profile.

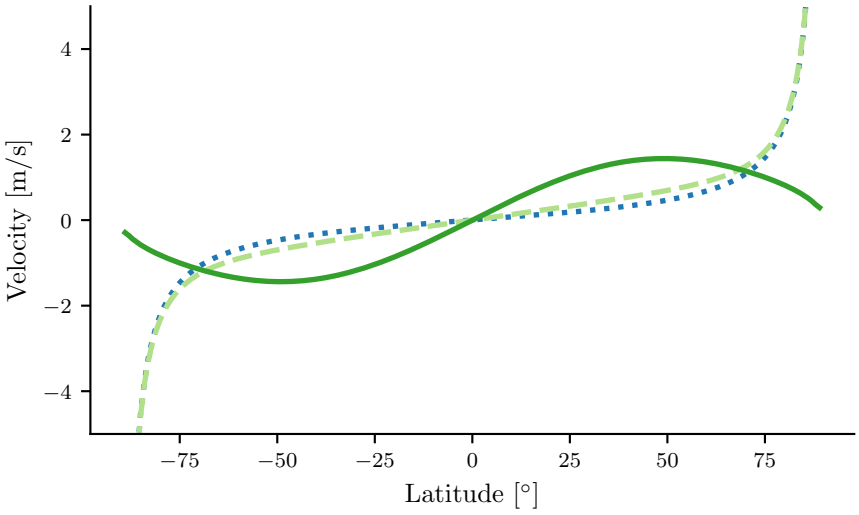

Figure 3.6: "Advection velocities" for three different models: dotted - constant tropopause height and diffusivity, dashed - non-uniform tropopause height and constant diffusivity, and solid - non-uniform tropopause height and diffusivity. The figure is cut off at $\pm 5\, ms^{-1}$, but reaches upward of $\pm 20\, ms^{-1}$ at the poles for the dotted and dashed lines.

CHAPTER 4

Results and discussion

As a baseline comparison between models, the temperature profiles of the different models developed and used in this thesis are presented in Figure 4.1. The solid line shows the zonal mean temperature of the surface pressure level of variable *ta* in NorESM2-LM, while the dashed and dotted lines shows the temperature profile shifted up by 30° C in the diffusion and MEP model, respectively. This was done as the temperature profiles in the idealized models represent a mean tropospheric temperature, which is generally colder compared with temperatures close to the surface. The incoming solar radiation is also less compared with NorESM2-LM (see Figure A.1). As can be seen in the figure, the idealized models generally exhibit similar temperature profiles as a fully-coupled ESM despite having no surface interactions nor clouds. The diffusion model underestimates tropical temperatures while overestimating temperatures everywhere else, while the MEP model underestimates polar temperatures, but shows high similarity everywhere else. Both of the idealized models have symmetric model parameters, and so the asymmetry between the poles is not present.

The diffusion model could potentially be tuned to fit the NorESM2-LM profile better, however, the goal of this comparison was only to assess a qualitative agreement, and so this was not done.

The total MHT was also calculated by integrating the net top of the atmosphere (TOA) radiation, see Donohoe, Armour et al., 2020 for details. Figure 4.2 shows the MHT in the different models. All of the models show a maximum in MHT at around 45°, which is what we would expect (Stone, 1978). The diffusion model follows the NorESM2-LM closely in the southern hemisphere (SH), but is generally slightly lower in the northern hemisphere (NH). As for the MEP model it is underestimating the MHT by about half almost everywhere. It is, however, important to consider that the TOA fluxes are lower for both idealized models, and that choosing a greater solar constant increases the heat transport in both models. The parameters were chosen before comparisons with NorESM2-LM was made, and the discrepancy in solar constant was not identified until the last stage of the writing process. In general, a comparison in MHT may not be a measure of validity as a climate model (Stone, 1978), but it is beneficial to confirm that they do agree in shape.

As a connection to our diffusion model, the diffusivity in NorESM2-LM (piControl) and the MEP model was estimated from the equilibrium diffusion

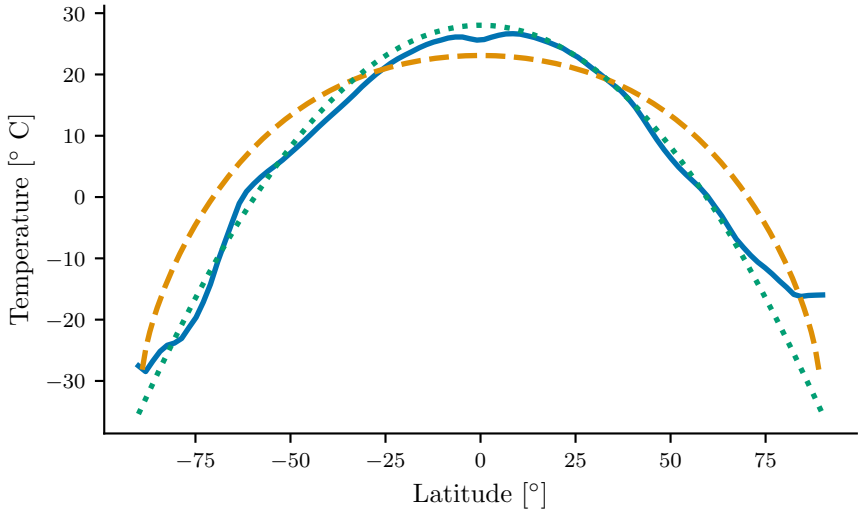

Figure 4.1: Meridional temperature profiles from: solid - NorESM2-LM, dashed - full complexity diffusion model, and dotted - maximum entropy production model. The NorESM2-LM-profile is of the highest pressure level (close to the surface), and the temperatures in the semi-analytical models are shifted by a constant 30° C to accommodate comparisons in shape.

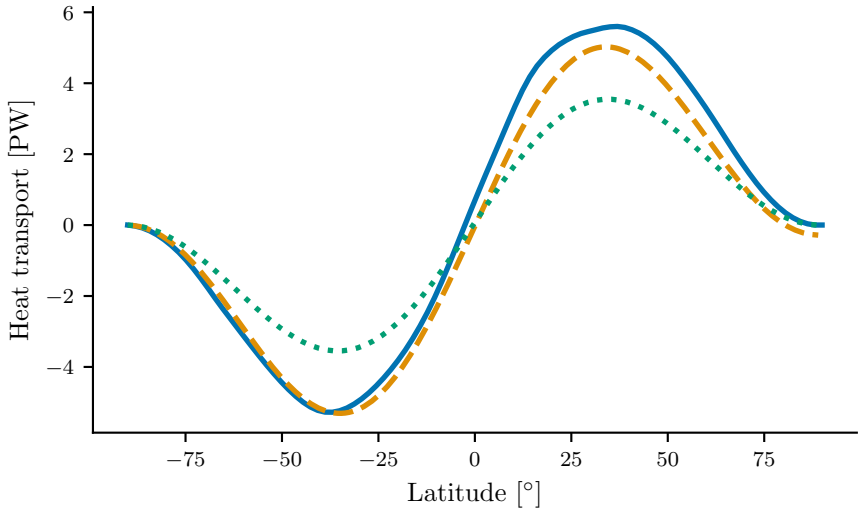

Figure 4.2: Meridional heat transports from: solid - NorESM2-LM, dashed - full complexity diffusion model, and dotted - maximum entropy production model.

model eq. (3.27). Due to the small values of heat flux and temperature gradient close to the equator, the calculation is numerically unstable in this region, and omitted. Following the same linestyle and colour scheme as earlier, Figure 4.3 shows the diffusivities for the different models. The diffusivity from the diffusion model was also calculated using the same method, and comparing the thin grey line and the dashed line, we can see that we get the expected diffusivity. Looking now at the MEP diffusivity (dotted line), we see that it is generally the lowest of the three, increasing equatorwards throughout most of the hemisphere until after 25° latitude where there is a very slight decline towards the equator.

The NorESM2-LM diffusivity profile is complex and exhibits hemispheric asymmetry. The NH has generally higher diffusivities and the maximum diffusivity of $10^7\,\mathrm{m^2 s}$ right next to the north pole. A curious feature which may be due to numerical instability, but then we would also expect similar behaviour at the south pole. Local maxima are present in the NH at around 50°N, 75°N, and equatorwards of 30° N the diffusivity increases, reaching a value of $3 \cdot 10^6\,\mathrm{m^2 s^{-1}}$ at 10°N. Similarly located maxima are present in the SH. This indicates that the maxima may be connected with the atmospheric cells in some way. The most interesting feature, however, is the pronounced minimum slightly south of 60°S which may be connected to the Antarctic Circumpolar Current and the prevailing westerlies. The diffusivity also decreases equatorwards of around 55°S in the SH, reaching a value of circa $1.8 \cdot 10^6\,\mathrm{m^2 s^{-1}}$ at 10°S. While the singularities near the equator might affect the values there, it is worthy to note that this asymmetry between high values in the NH and low values in the SH is present in the diffusivities used by Sellers, 1969.

Throughout the rest of this chapter we will focus on results from the idealized models. A number of different diffusion model complexities will be studied, all listed below, and will be referred to as "model number 1" etc. Higher numbers represent higher model complexity, i.e. spherical geometry vs. cartesian geometry, non-uniform tropopause height vs. constant tropopause height etc. Additionally, while the effect of chosen geometry in a model with non-uniform diffusivity could be studied, this was not done due to only keeping linear terms in the model derivation, and so cross-effects are not expected.

1. dashdotted - cartesian geometry with constant tropopause height and diffusivity
2. dotted - spherical geometry with constant tropopause height and diffusivity
3. dashed - spherical geometry with varying tropopause height and constant diffusivity
4. solid green - spherical geometry with varying tropopause height and diffusivity

Additionally, the MEP model only represents one model complexity with linestyle and color solid blue.

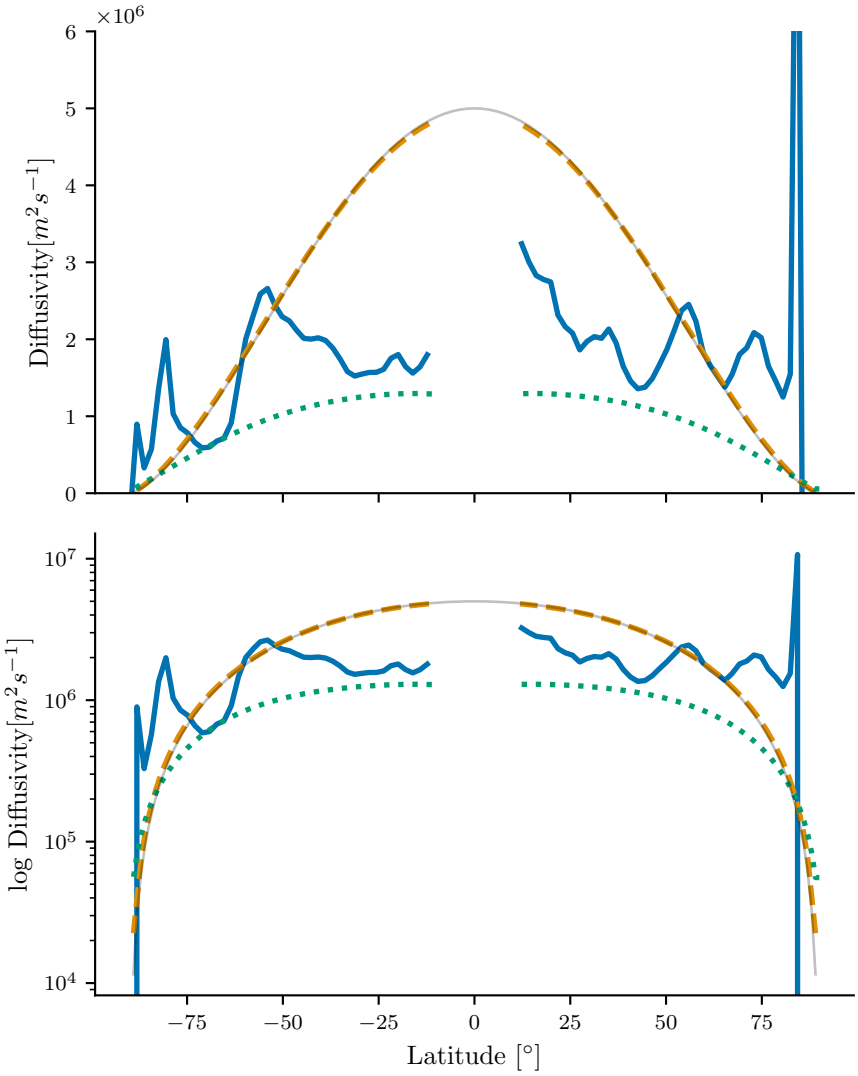

Figure 4.3: Estimate of diffusivity assuming a tropopause height as in Figure 3.5c derived from eq. (3.27) for linear scale (upper) cut-off at $6 \cdot 10^6\ m^2 s^{-1}$ and semi-logarithmic (lower). solid - NorESM2-LM, dashed - full complexity diffusion model, and dotted - maximum entropy production model. The solid grey line is the prescribed diffusivity (eq. (2.9)). Latitudes within ±10° are not shown due to singularities close to the equator.

4.1 Emissivity

Figure 4.4 shows the emissivity decrease equilibrium response of the models. This was done to assess the baseline temperature response to GHG emissions without any additional perturbations.

Temperature anomalies in models 1, 2, and 3 are similar in shape, exhibiting slight TA , but model 1 generally shows lower magnitudes of around 0.05°. This is due to the difference in total volume between the cartesian and spherical models. Spherical geometry slightly alleviates TA, reducing the poleward gradient, but not enough to break even or produce PA. Accounting for a lower tropopause in polar areas has a negligible effect on the temperature anomaly, which might be expected when comparing horizontal and vertical scales. I.e. we would expect that accounting for varying surface area has a larger impact compared with accounting for a non-uniform tropopause, which looks to be the case. Model 4 illustrates the effect of a latitudinally varying diffusivity profile and the temperature anomaly is markedly different from all previous models showing smaller gradients equatorward of 50° latitude and a sharp decline poleward of 50°, again showing TA (the largest, of around 0.10°C). This is consistent with the theoretical temperature anomaly from an emissivity perturbation in the continuous and two box models (see Section 3) and the effect of decreasing diffusivity polewards.

Similarly, the MEP model also exhibits TA, and the temperature anomaly is comparable to the diffusion models in magnitude. However, the temperature difference between tropical and polar areas is significantly larger (around 0.30°C) and there is a sharp gradient polewards of the tropics.

Additionally, the temperature anomaly relates to the temperature profile by eq. (3.29). The smaller temperature contrasts in the constant diffusivity spherical models may then be interpreted as being due to the monotonically increasing "advection" velocities poleward, while in model 4 the "advection" velocities peak in the mid-latitudes, decreasing polewards. This is reflected in model 4 by small temperature contrasts between the tropics and mid-latitudes, but sharp decline towards the arctic.

All of our models show TA under emissivity decrease which is also consistent with another dry diffusive EBM by Armour et al., 2019. Introducing latent heat exchanges in this model produced PA instead, and so the baseline response of TA may simply be a case of missing physics in our models.

4.2 Albedo

Figure 4.5 shows the temperature response to a uniform decrease in albedo by $\Delta\alpha = -0.01$. The responses of the diffusion models all exhibit TA with the maximum tropical warming shown in the cartesian model 1, contrary to the temperature anomaly for a emissivity decrease, where the spherical models exhibited strongest TA. Model 4 shows the largest temperature difference between the tropics and poles for all models, while models 2 and 3 have similar polar warming to model 1, but decreased TA. Looking back at eq. (3.29) it seems the solar constant dominates the albedo-term due to the model showing

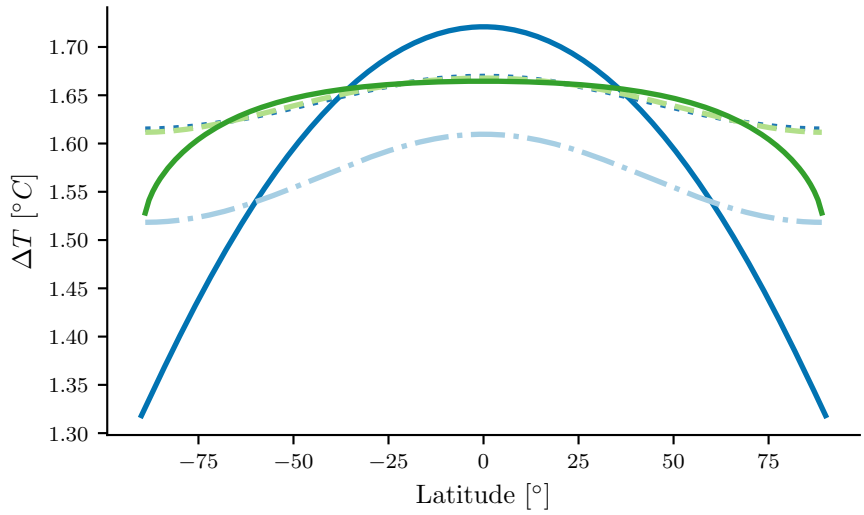

Figure 4.4: Equilibrium temperature anomalies for a emissivity perturbation $\Delta\epsilon = -0.02$ *for dashdotted - cartesian geometry and constant tropopause and diffusivity, dotted - spherical geometry and constant tropopause height and diffusivity, dashed - spherical geometry with non-uniform tropopause height and constant emissivity, and solid green - spherical geometry with non-uniform tropopause height and diffusivity, solid blue - maximum entropy production model.*

TA. This also makes sense physically, as the tropics is the region of most incident solar radiation and largest surface area, and so a lowering of the albedo traps more heat here than compared with the poles.

The MEP model shows non-trivial behaviour, maximizing the temperature anomaly around 75° around 1° C before decreasing polewards. A minimum is present in the tropics just above 0.9° C, where the temperature anomaly is comparable to that just at the poles. In general, the temperature differences are not very large in the MEP model. A possible explanation may be that the MEP model maximizes the heat transport, and so the excess heat in the tropics is efficiently transported polewards.

Considering a more realistic scenario of albedo change, that of arctic sea ice melt, the temperature response to a decrease in albedo northwards of 80° N is shown in Figure 4.6 for the same models as earlier. All the models exhibit PA. For the diffusion models, there is a decrease in PA when comparing the cartesian model 1 with spherical models 2 and 3, which may be caused by the decreased surface area in this region in the spherical models. Again a non-uniform tropopause height has a negligible impact on the temperature anomaly. Letting the diffusivity vary latitudinally in model 4, with decreasing diffusivity polewards, increases polar temperatures significantly compared with all earlier diffusion models, reaching a maximum of around 0.60 ° C at the north pole. All diffusion models exhibit non-local effects due to local albedo decrease, presumably due to diffusion, which spreads out the signal. This is especially

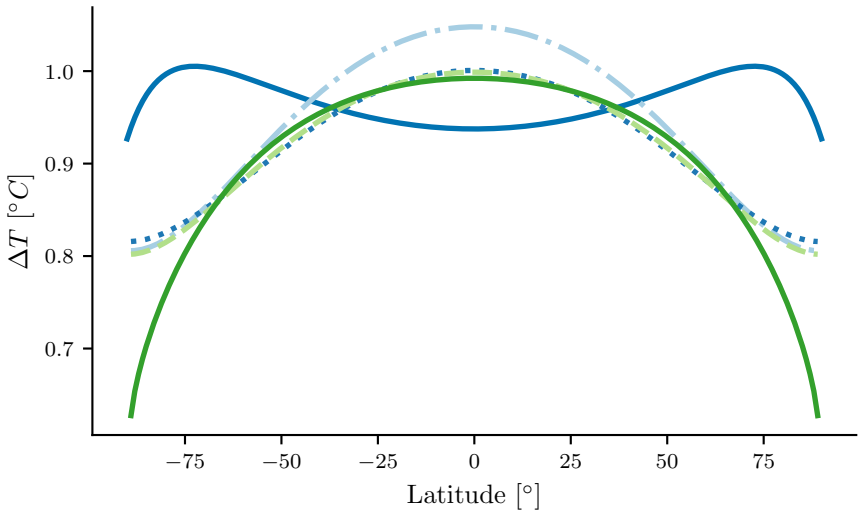

Figure 4.5: Equilibrium temperature anomalies for a globally uniform albedo decrease of $\Delta\alpha = -0.01$ for dashdotted - cartesian geometry and constant tropopause and diffusivity, dotted - spherical geometry and constant tropopause height and diffusivity, dashed - spherical geometry with varying tropopause height and constant emissivity, and solid green - spherical geometry with varying tropopause height and diffusivity, solid blue - maximum entropy production model.

apparent in model 1 where the temperature anomaly is affected throughout the entire NH and perhaps even slightly in the SH. In the spherical models 2, 3, and 4 this effect is mostly contained to the NH mid-latitudes. For models 2 and 3 this may simply be due to the smaller maximum at the pole compared to model 1, however, for model 4 this is not the case as the polar maximum is larger. The significantly smaller diffusivities (Figure 3.5 d) throughout the mid-latitudes may be the cause of the reduced non-locality of polar albedo decrease. Albedo decrease in the arctic reduces the northward MHT (Figure A.3), which is expected due to the reduced temperature gradient.

This is not at all the case for the MEP-model, where there is an abrupt increase in temperature at 80°N reaching a maximum of 1.75°C there and decreasing northwards. The last decrease may be due to the weakening solar constant polewards. This may imply equatorward diffusion of heat. The MHT barely changes for the MEP model in this scenario (Figure A.3).

4.3 Tropopause height

The tropopause has been observed to heighten in observations (Santer et al., 2003), as well as ESMs (Vallis et al., 2015). Due to the relatively modest volumetric effects from spherical geometry, it was then natural to investigate the volumetric effects due to THI. As shown in Chapter 3, the MEP model temperature anomaly is unaffected by the tropopause height, and so is not

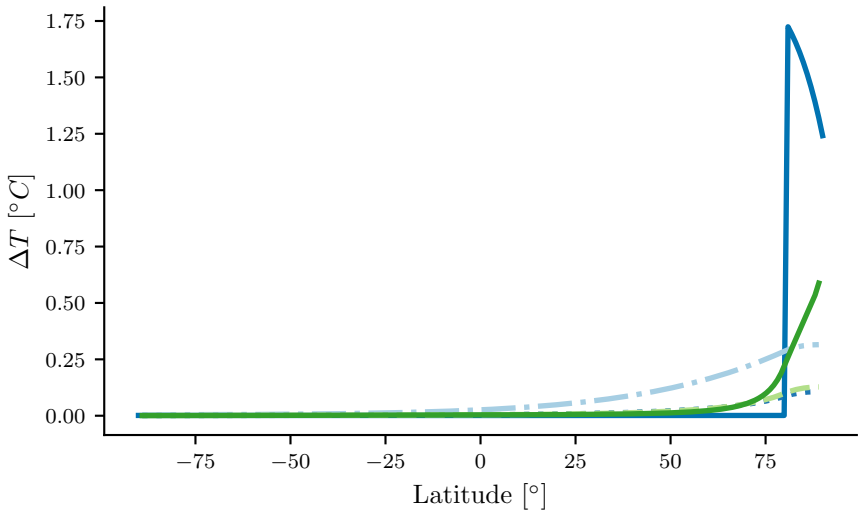

Figure 4.6: Equilibrium temperature anomalies for a local albedo perturbation $\Delta\alpha = -0.04$ *northwards of* $80°$ *latitude for dashdotted - cartesian geometry and constant tropopause and diffusivity, dotted - spherical geometry and constant tropopause height and diffusivity, dashed - spherical geometry with varying tropopause height and constant emissivity, and solid green - spherical geometry with varying tropopause height and diffusivity, solid blue - MEP model.*

included in the following figures. The temperature anomalies for models 1-4 due to THI are shown in Figure 4.7. There is a slight cooling in the tropical region with significantly more heating at higher latitudes, peaking at the poles in all models. The tropical cooling is largest in the cartesian model. While the temperature anomalies in constant diffusivity models are similar, the non-uniform diffusivity model shows a significantly larger and sharper temperature increase in the polar regions.

The PA and tropical cooling seen here are consistent with the continuous and two box models discussed previously. Diffusion is reducing the temperature contrasts present in the TOA. Essentially, PA due to THI is only relevant as a diffusion phenomenon. Eq. (3.32) shows that THI has a cooling effect wherever there is radiative convergence and a heating effect wherever there is radiative divergence. THI increases the poleward MHT, and so the excess heat in the tropics is transferred towards the arctic (Figure A.2)

Figure 4.8 illustrates the diffusivity dependence of combined emissivity and height perturbation in a constant diffusivity spherical model. For low diffusivities the temperature anomaly is tropically amplified, and increasing the diffusivity, the temperature anomaly shifts towards being amplified at the poles until a point $D = 10^8 \mathrm{m}^2\mathrm{s}^{-1}$ where the temperature anomaly flattens out. Thus, the temperature anomaly is a non-monotonic function of diffusivity under emissivity and height perturbations, which is consistent with the approximate temperature anomaly in the intermediate diffusion case of the continuous model and the exact expression in the two box model.

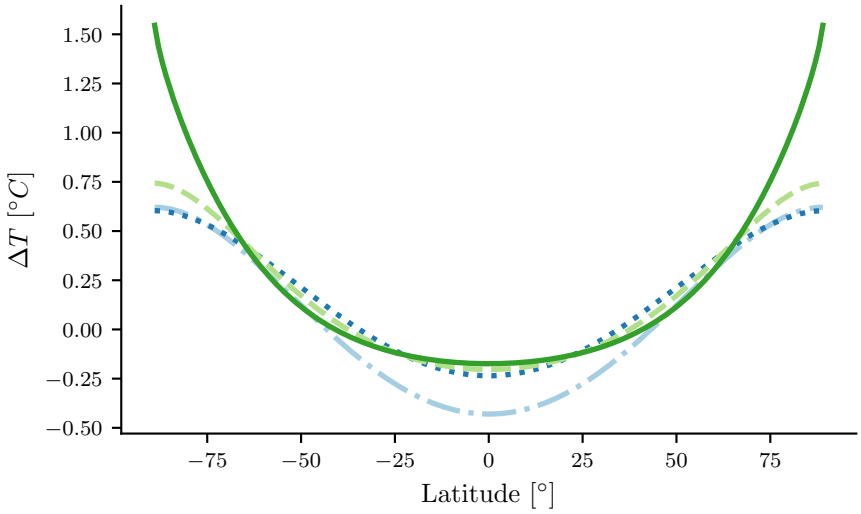

Figure 4.7: Equilibrium temperature anomalies for a uniform tropopause height perturbation $\Delta H = 300m$ for dashdotted - cartesian geometry and constant tropopause and diffusivity, dotted - spherical geometry and constant tropopause height and diffusivity, dashed - spherical geometry with varying tropopause height and constant emissivity, and solid - spherical geometry with varying tropopause height and diffusivity.

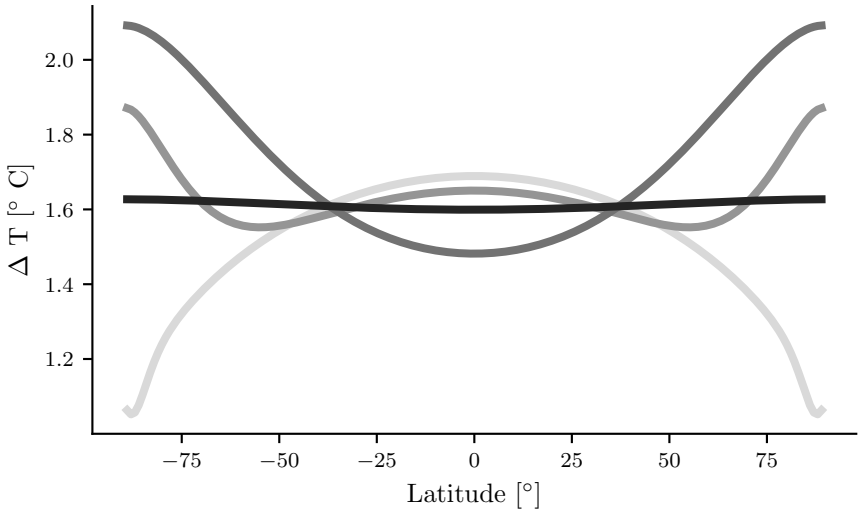

Figure 4.8: Equilibrium temperature anomalies due to a emissivity perturbation $\Delta\epsilon = -0.02$ and height perturbation $\Delta H = 300$ m for increasing diffusivity, where lighter shades of grey denotes lower diffusivites in a range $D \in [10^3, 10^8]\, m^2 s^{-1}$.

Exploration of Asymmetric Polar Amplification

PA is mostly observed in the Arctic, as noted previously. In the MEP model this would realistically be due to an asymmetry in albedo decrease, while in the diffusion models a THI may contribute. We therefore explore hemispheric asymmetry in model 4 as seen in Figure 4.9 and can be summarized in the following three scenarios:

- Scenario i: the tropopause height is reduced by 2500 m over the Antarctic continent resulting in a temperature anomaly around 0.4°C larger compared with the Arctic.
- Scenario ii: in addition to tropopause height reduction as in scenario i, THI is also larger in the Antarctic region, as suggested in Vallis et al., 2015, Figure 7a, which causes a slight additional warming of 0.1° C.
- Scenario iii: including both previous changes, the diffusivity is set to rapidly decay over the Antarctic continent, which results in significantly reduced warming compared with previous scenarios and the Arctic, yet still larger compared with lower latitudes. As any warming goes to zero with diffusivity, any PA here reflects a non-zero diffusivity. The decaying function used was the following:

$$f = 5 \cdot 10^6 \exp((\theta + 70\pi/180)). \tag{4.1}$$

The results from scenario i are expected due to the slight increase in PA from a non-uniform tropopause height as seen in Figure 4.7 model 2 - 3. A physical explanation can be that there is simply less air to heat up in this region, therefore causing amplified warming. L. Hahn et al., 2019; L. C. Hahn et al., 2020 argues that the elevation of the Antarctic continent is the cause of asymmetry in PA due to its effect on the lapse-rate feedback in the region. Similarly, our model shows that not considering the elevation difference results in symmetric PA, although admittedly, the observed asymmetry is of lesser Antarctic Amplification, not more as in our model. Our model does, however, not simulate the lapse-rate feedback although the tropopause height is dependent on the lapse-rate (Hu and Vallis, 2019).

Scenario ii illustrates the effectiveness of increased THI compared to a lower tropopause height as the THI is only by 150 m while the elevation difference is 2500 m.

Another effect that might cause asymmetry in PA is reduced diffusivity in the Antarctic region, which can, as demonstrated in scenario iii, have drastic consequences for the temperature anomaly in the region. The rapidly decreasing diffusivity in the Antarctic region also looks to have non-local effects on the entire SH and even the NH, although miniscule, as seen from the generally reduced temperature anomalies almost everywhere.

4.4 The relative importance of the different perturbations

As (e.g.) Figure 4.7 and 4.8 illustrates, perturbation effects are dependent on the distribution and magnitude of diffusivity, and so a realistic diffusivity profile

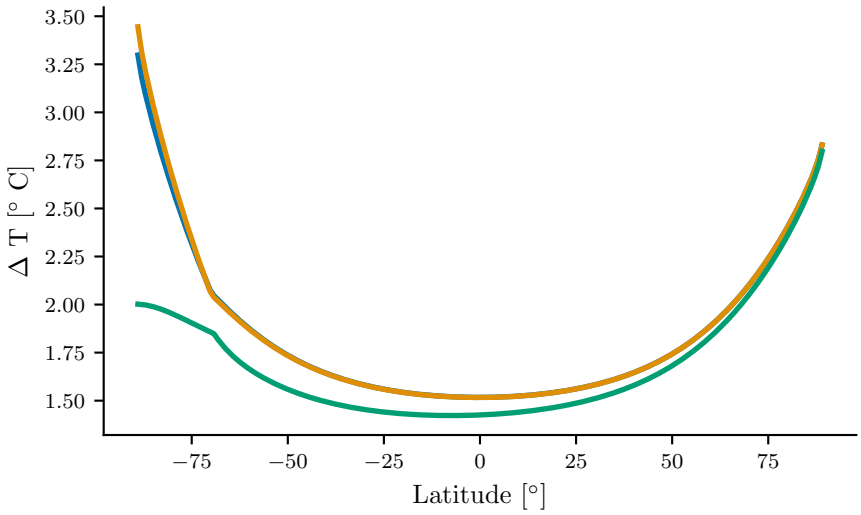

Figure 4.9: Different scenarios of tropopause height change accounting for asymmetries at the Antarctic. blue - reduced tropopause height poleward of 80 ° S by 2500 m, orange - Increased tropopause height change by 50 m in the same latitude range, green - Exponential decay of diffusivity in the Antarctic region.

is necessary to quantitatively compare the effects. A qualitative comparison can however be made by calculating the PAF for different possible perturbations as a function of diffusivity, which is shown in Figure 4.10. All perturbations converge to uniform warming at higher diffusivities (10^7 - 10^8)$\mathrm{m^2 s^{-1}}$. A decrease in emissivity causes slight TA for low and intermediate diffusivity, while a negative albedo perturbation in the Arctic region causes significant PA for low and intermediate diffusivities. Increasing the tropopause height alongside decreasing emissivity causes more TA for an diffusivity $D = 10^3\,\mathrm{m^2 s^{-1}}$ before contributing to PA with increasing magnitude after $D = 10^4\,\mathrm{m^2 s^{-1}}$. In the region $D \in (10^5, 10^7)\,\mathrm{m^2 s^{-1}}$ a THI contributes significantly to PA with maximum effect around $10^6\,\mathrm{m^2 s^{-1}}$. Including all perturbations, the PAF is dominated by the albedo perturbation for most diffusivities, except in the range $D \in (10^6, 10^7)\,\mathrm{m^2 s^{-1}}$ where the tropopause height perturbation and albedo perturbation contributes comparably. This region is close to observations of the diffusivity as done by Thiebaux, 1976 who found a value $D = 3 \cdot 10^7 \mathrm{m^2 s^{-1}}$ based on balloons. Important to note is that the magnitude of arctic albedo change is based on observations by Pistone et al., 2014 over roughly three decades (1979-2011), while the magnitude of THI is extrapolated from the National Centers for Environmental Prediction (NCEP) data used in Santer et al., 2003 that showed a THI of roughly 190 m in the period 1979-1999.

As a comparison, the PAF for an identical albedo perturbation was calculated for the MEP model. The mean MEP diffusivity was estimated by eq. (3.27) using a weighted average, excluding latitudes within 15° in both hemispheres, and the resulting PAF is significantly greater compared to that of the diffusion model for the same diffusivity. This is consistent with the abrupt and significant increase in temperature as seen in Figure 4.6.

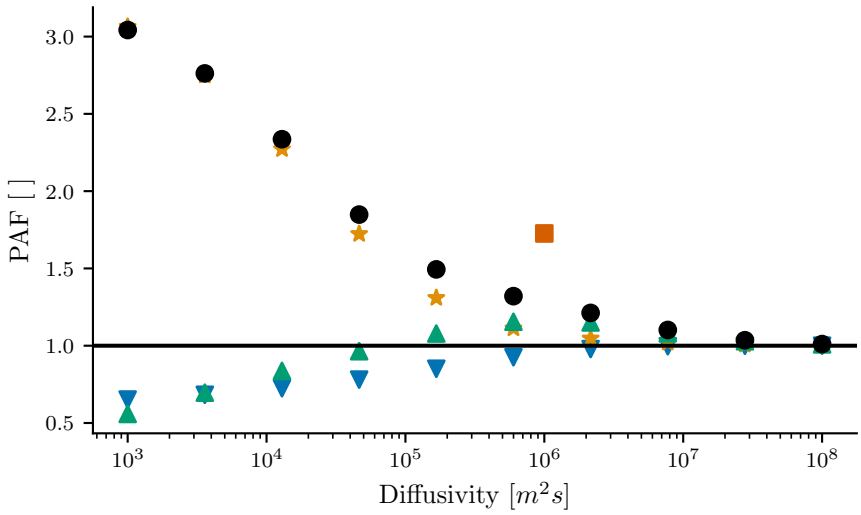

Figure 4.10: Polar Amplification Factor for different types of perturbations in a constant diffusivity model. Down triangle - $\Delta\epsilon = -0.02$ everywhere, star - $\Delta\alpha = -0.04$ polewards of $80°$ N and $\Delta\epsilon = -0.02$ everywhere, up triangle - $\Delta H = 300$ m and $\Delta\epsilon = -0.02$ everywhere, ***circle*** *- all perturbations, and square - maximum entropy production model $\Delta\alpha = -0.04$ polewards of $80°$ N and $\Delta\epsilon = -0.02$.*

4.5 Diffusivity

A major assumption in the diffusion model is that the form and magnitude of diffusivity is specified. Fourier's law (eq. (2.8)) implies that the diffusivity of the troposphere may change due to changes in meridional heat flux and temperature gradient. The diffusivity plays a similar role mathematically as the tropopause height in the diffusion operator (eq. 3.26), and repeating the perturbation analysis for the diffusivity in the intermediate diffusivity case would yield a similar contribution to the temperature anomaly as for a tropopause height perturbation. In light of the MEP model where THI has no effect on the temperature anomaly, this might offer a plausible explanation in form of a simultaneous diffusivity decrease (DD), which essentially mirrors the temperature anomaly in Figure 4.7. This is illustrated in Figure 4.11 where a DD of 1% was applied. In the non-uniform diffusivity case, this decrease was proportional to the diffusivity distribution (Figure 3.5 d), which was done due to the large magnitude difference between high and low latitudes. Figure 4.11 shows that increasing the complexity of the model tends to decrease tropical heating, whereas in Figure 4.7 this tended to decrease the tropical cooling, showing mirroring, as expected.

Figure 4.12 shows the PAF as a function of THI and DD in model 2 where an emissivity decrease of $\Delta\epsilon = -0.02$ was applied to ensure the PAF is well-defined. An essentially linear relationship between tropopause height and diffusivity is found, implying that any potential non-linear terms ($\Delta D \Delta H$) have little to no effect on the temperature anomaly. For larger perturbations than

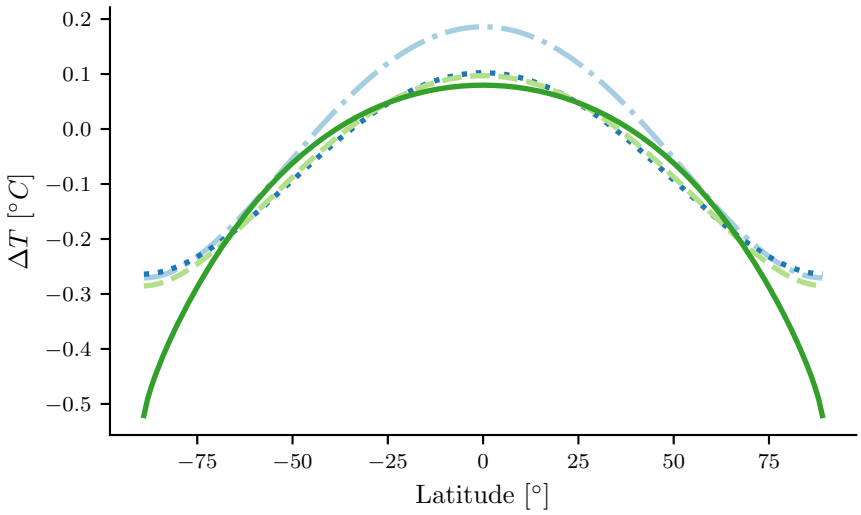

Figure 4.11: Equilibrium temperature anomalies due to a relative diffusivity decrease of $\Delta D/D = -1\%$ for dashdotted - cartesian geometry and constant tropopause and diffusivity, dotted - spherical geometry and constant tropopause height and diffusivity, dashed - spherical geometry with varying tropopause height and constant emissivity, and solid - spherical geometry with varying tropopause height and diffusivity.

are shown here, this may not hold as the non-linear terms could potentially become significant. The gray area denotes the regime where THI induced PA is essentially cancelled by TA due to DD. As the PAF does not show the actual shape of the temperature anomaly, the temperature anomaly was plotted for a select tropopause height and diffusivity perturbation (Figure A.4), and while the figure does not show exact uniform warming, achieving this would require significantly more model runs, and the discrepancy between the poles and the tropics is on the order of $\mathcal{O}(10^{-3})$.

Additionally, Figure 4.12 lets us estimate the percentage diffusivity decrease needed to counteract PA by a 2.4% THI, yielding a relative DD, $\Delta D/D \approx -2\%$.

In the MEP model, the tropopause height has no effect on the temperature anomaly, however, the heat fluxes are still affected due to their dependence on the cross-sectional area S, thus the diffusivity is changed when changing the tropopause height. Calculating the diffusivity, as done in Figure 4.3, for two model runs, one with baseline height and one with increased tropopause height, the diffusivity anomaly due to a THI of $\Delta H = 300\,\mathrm{m}$ is shown in Figure 4.13. We can see a negative anomaly across the globe with the largest decrease towards the tropics. The mean global decrease is of around $\Delta D/D \approx -2.4\%$, which is roughly consistent with the diffusivity decrease required to balance the effect of THI in model 2. As the temperature distribution, and therefore the MHT, is unaffected by the tropopause height in the MEP model, the heat fluxes must necessarily decrease when the tropopause increases, which is how the

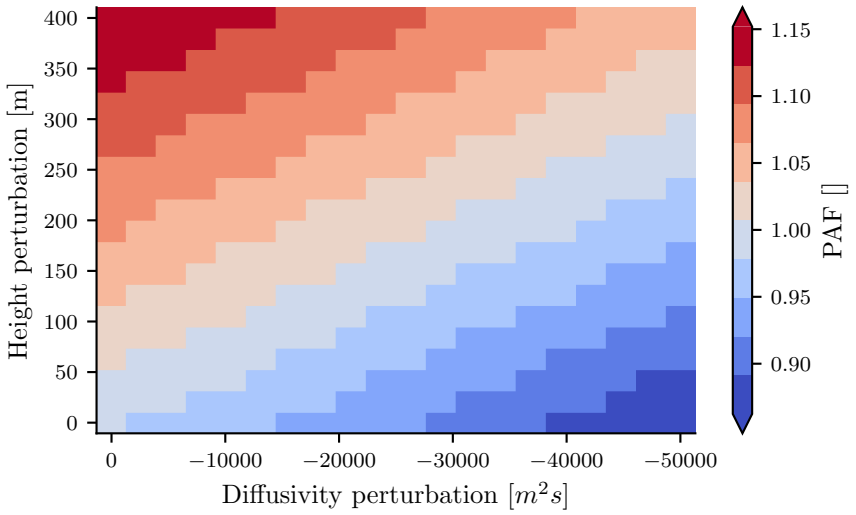

Figure 4.12: Polar amplification factor as a function of tropopause height and eddy diffusivity perturbations in a spherical model with constant tropopause height and eddy diffusivity. Red shading indicates polar amplification while blue shading indicates tropical amplification.

DD anomaly is calculated. In terms of Fourier's law (eq. (2.8)) the diffusivity perturbation as function of a tropopause height perturbation is

$$\frac{\Delta D}{D} = -\frac{\frac{\Delta H}{H}}{1 + \frac{\Delta H}{H}}, \tag{4.2}$$

which lends further credency to DD as a compensating mechanism for THI.

Stone, 1978 argued that changes in incoming solar radiation and albedo are the primary drivers of change to the MHT, which is consistent with the MEP model, but not the diffusion models as tropopause height is clearly affecting the MHT. Either Stone's model is too simple (not accounting for tropospheric geometry) or a mechanism such as DD acts against THI, essentially balancing the effects.

As mentioned previously, the diffusivity might change under GHG-forcing. Perturbing Fourier's law (eq. (2.8)) in heat transport and tropopause height yielded

$$\frac{\Delta D}{D} = \frac{\frac{\Delta Q}{Q} - \frac{\Delta H}{H}}{1 + \frac{\Delta H}{H}}.. \tag{4.3}$$

Using an available measure of the change in MHT in an ensemble of ESMs provided by Donohoe, Armour et al., 2020 ($\Delta Q = 0.1\,\mathrm{PW}$), as well as a measure of THI found by Hardiman et al., 2019 ($\Delta H \approx 1500\,\mathrm{m}$) under the same $4xCO_2$-scenario in HadGEM3-GC3.1 we can compare the relative contributions of the

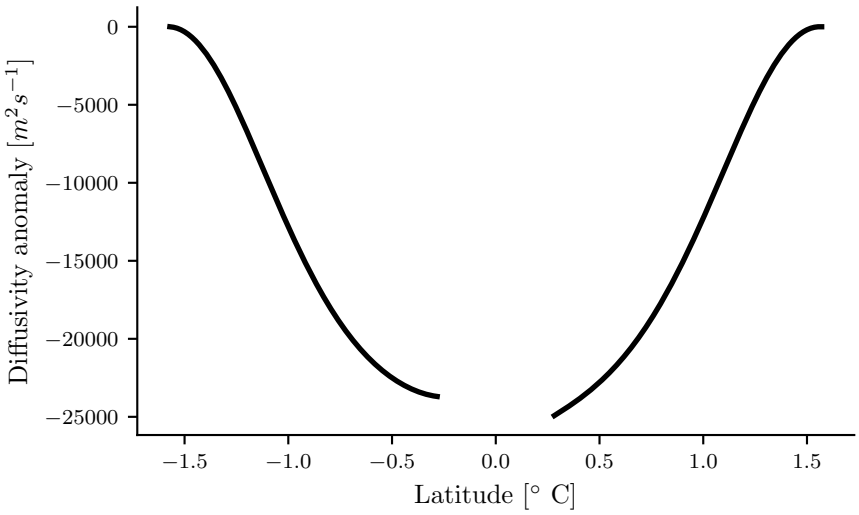

Figure 4.13: Diffusivity anomaly in a maximum entropy production model for a tropopause height increase of $\Delta H = 300\,m$.

two effects:

$$\frac{\Delta Q}{Q} = \frac{0.1}{4} = 2\,\%$$
$$-\frac{\Delta H}{H} = -\frac{1500}{12500} = -12\,\%.$$

The implied DD due to THI is a lot larger than the diffusivity increase du to an increase in the MHT. However, the temperature gradient could also change, contributing to a change in diffusivity. Gitelman et al., 1997 looked at trends in the meridional temperature gradient, and found a steady decline, which would contribute to diffusivity increase. A more careful study is needed to study the mechanisms of THI and DD.

CHAPTER 5

Conclusions

5.1 Main findings

Our work investigated the effect of geometry on the distribution of heating in the atmosphere due to greenhouse gas emissions in two types of energy balance models (EBMs): a dry diffusion model and a maximum entropy production (MEP) model. In response to a decrease in planetary emissivity, the baseline temperature response to greenhouse gas (GHG) emissions was found to be that of tropical amplification (TA). In the diffusion model, accounting for spherical geometry had a significant impact on the magnitude of warming due to the overall smaller volume, however, while slightly more heat was redistributed towards the poles due to "advection" of temperature, this effect was not great enough to counteract TA. A further geometric consideration was made, that of a non-uniform tropopause height. This had only an negligible effect on the temperature anomaly which was consistent with an almost identical temperature "advection" velocity as in the case for spherical geometry with a constant tropopause height. Having a non-uniform diffusivity was also explored, which caused the strongest TA of the diffusion models. The MEP model produced the largest TA, however, and it was shown analytically that the temperature anomaly in this model was independent of geometry.

Due to the modest polar amplification (PA) signal from accounting for the geometry of the troposphere, more possible mechanisms were explored:

- Arctic sea-ice melt, represented by decreasing arctic albedo, caused PA in all models with the largest magnitude of PA in the MEP model. The response in the diffusion and MEP models were qualitatively different, while the MEP model showed an abrupt temperature increase in the arctic only, the diffusion models exhibited non-local effects, altering the meridional heat transport (MHT) due to the change in the temperature gradient and therefore the temperature anomaly throughout the entire northern hemisphere (NH).

- Tropopause height increase (THI) yielded a PA response in all diffusion models which strength was found to be dependent on the magnitude of diffusivity in a uniform diffusivity model. For realistic values of the diffusivity, the Polar Amplification Factor (PAF) was similar to that of arctic albedo decrease using realistic estimates of THI and albedo

decrease due to sea ice melt. In a non-uniform diffusivity model, a locally reduced magnitude of diffusivity over Antarctica had drastic effects on the temperature anomaly, reducing THI induced PA significantly and reduced warming throughout most latitudes, exhibiting non-locality. This effect was not present in the MEP model due to the aforementioned non-dependence on geometry.

- A change in diffusivity was found to have a mathematically identical effect as a change in tropopause height in the equilibrium diffusion model, and so a possible mechanism contributing to PA. However, due to a opposite sign relationship between a diffusivity perturbation and a tropopause height perturbation in Fourier's law, a possible compensating mechanism reconciling the diffusion models and the MEP model was identified - that of diffusivity decrease (DD). DD due to an increased tropopause height but constant MHT in the MEP model was consistent with the DD needed to counteract PA due to THI in the diffusion model. The MEP model maximizes the heat transport, and any change in the cross-sectional area S must then be balanced by the heat flux.

All of these mechanisms, including the effect of non-equal volumes, were also represented in a continuous equilibrium model as well as an analytically solvable two box model, which was the simplest possible representation.

The diffusivity in earth system models (ESMs) was also investigated. Estimating the diffusivity using an equation derived from the equilibrium diffusion model proved unfeasible in the tropics due to numerical singularities there, however, an estimate was found for the extratropics which was similar in magnitude to that of the diffusion and MEP models. An estimate of the change in diffusivity due to quadrupling of CO_2 was made using Fourier's law yielding a large DD. The estimate was dominated by THI, with only an increase in MHT contributing positively. A potential change in the meridional temperature gradient may also contribute positively.

5.2 Further research

Additional work can be done to investigate the validity of THI as a mechanism for PA.

An ESM ensemble study could be conducted where the mechanism of heat transport change was further explored. Does THI affect the MHT in an ESM, or is Stone, 1978 correct that only albedo change significantly alters the MHT? Additionally, a method of calculating diffusivities including the tropics could be developed which would let us find the complete ensemble eddy diffusivity profile of the atmosphere and the anomaly due to GHG emissions. From this we could also calculate the correlation between DD and THI in the models, which can potentially confirm if a increase in tropopause height is compensated by a decrease in diffusivity. It could also be that there is an increase in diffusivity, which the diffusion models suggests would yield PA. The magnitude of this potential increase would let us compare PAF with albedo decrease and THI.

Additionally, an idealized model with an active surface could be developed in which the tropopause height is dependent on the surface interaction. This could potentially investigate if the lapse-rate feedback is sufficient for PA or if THI is required. Developing a most-static energy model to investigate the results from this thesis could be another direction to go. These models yield a baseline PA signal, and may be a better representation of the phenomenon in general.

More understanding could be extracted from the MEP model by applying the equilibrium perturbation approach. Another natural direction of further study is expanding on the MEP model. Simulating multiple interacting vertical layers could open possibilities to explore the tropopause height in way of a thermal tropopause akin to a model developed by Pujol and Fort, 2002.

All in all, the models in this thesis are highly idealized and there are many avenues for further exploration of the mechanisms of PA identified and explored. Especially the mechanism of THI induced PA could challenge the view that only incoming solar radiation and albedo are the main contributors to the MHT as argued by Stone, 1978.

Appendices

APPENDIX A

Additional figures

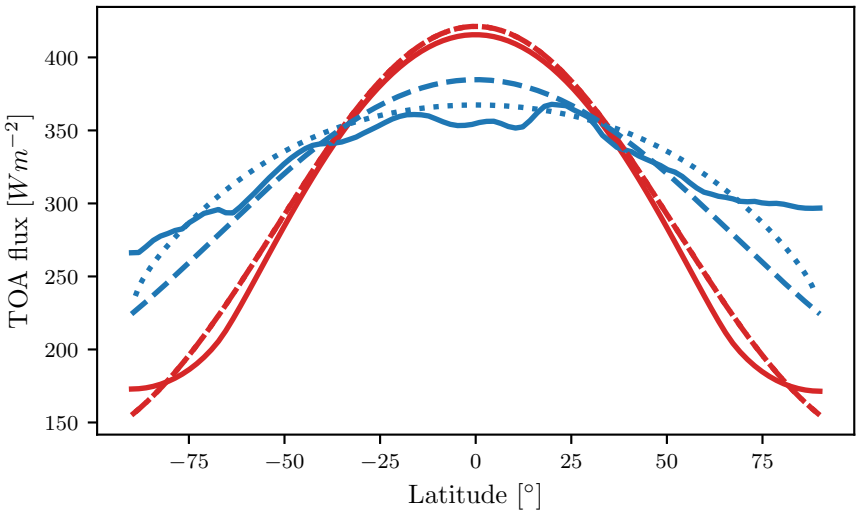

Figure A.1: Incoming and outgoing radiative fluxes for solid - NorESM2-LM, dashed - full complexity diffusion model, and dotted - maximum entropy production model. The profiles from the idealized models are shifted by a constant 140 Wm^{-2} *for easy comparison.*

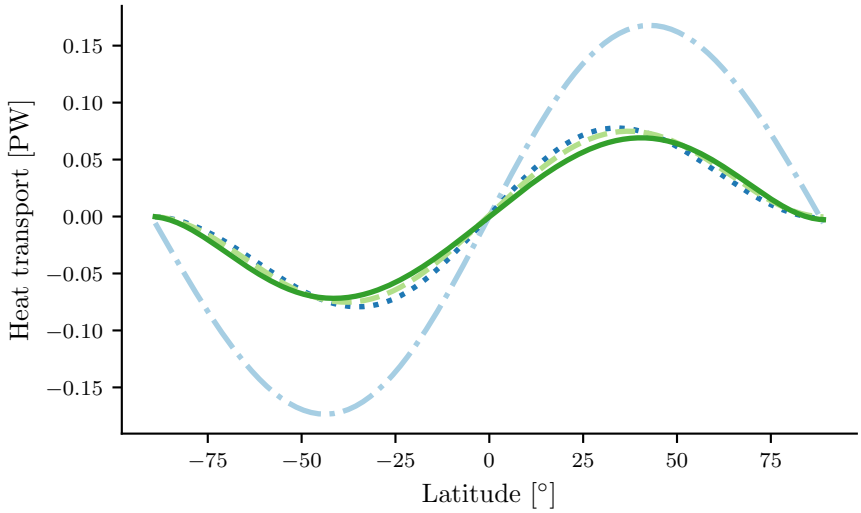

Figure A.2: Heat transport anomalies for a tropopause height increase of $\Delta H = 300\,m$ *for dashdotted - cartesian geometry and constant tropopause and diffusivity, dotted - spherical geometry and constant tropopause height and diffusivity, dashed - spherical geometry with varying tropopause height and constant emissivity, and solid green - spherical geometry with varying tropopause height and diffusivity.*

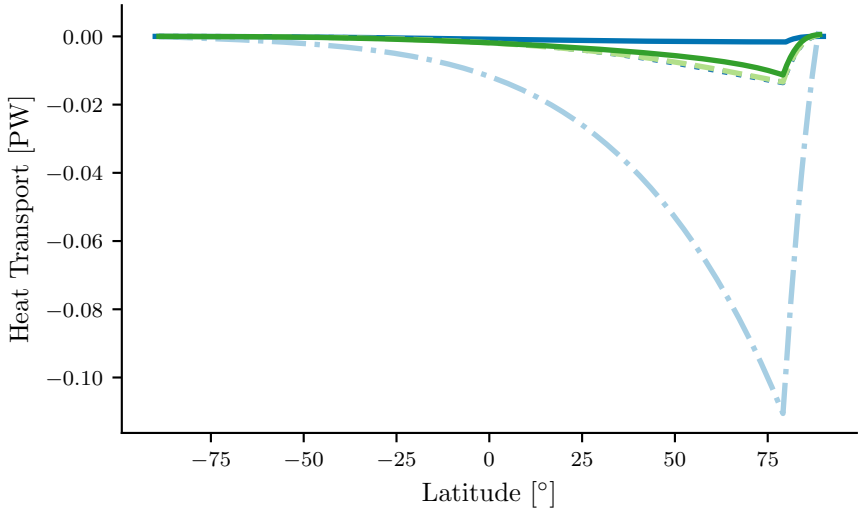

Figure A.3: Heat transport anomalies for an albedo decrease of $\Delta\alpha = -0.04$ *northwards of* $80°$ *N for dashdotted - cartesian geometry and constant tropopause and diffusivity, dotted - spherical geometry and constant tropopause height and diffusivity, dashed - spherical geometry with varying tropopause height and constant emissivity, and solid green - spherical geometry with varying tropopause height and diffusivity, solid blue - maximum entropy production model.*

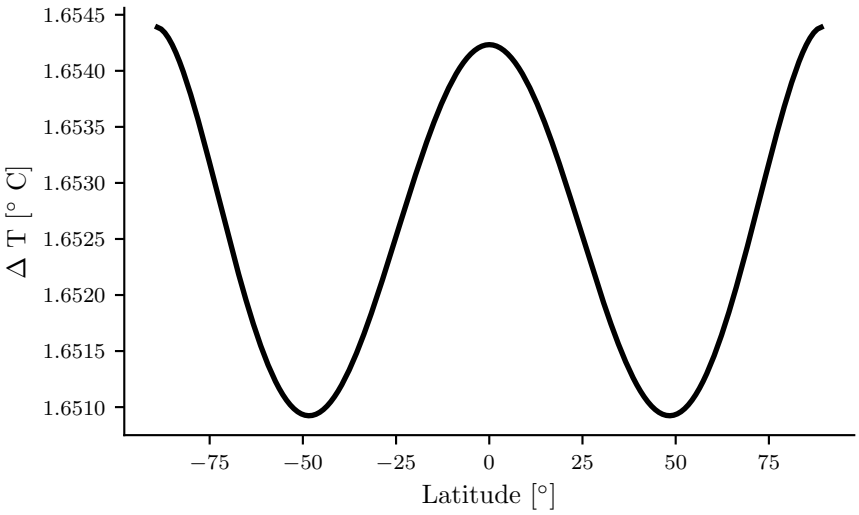

Figure A.4: Temperature anomaly for simultaneous tropopause height increase of $\Delta H = 250\,m$ and diffusivity decrease of $4.16 \cdot 10^4\,m^2 s^{-1}$ for a spherical diffusion model with constant tropopause height and diffusivity.

APPENDIX B

Equations and derivations

B.1 Equations

Trigonometric equations

Trigonometric addition rule for cosines

$$\cos(\theta + \phi) = \sin\theta \sin\phi - \cos\theta \cos\phi \tag{B.1}$$

Trigonometric addition rule for sines

$$\sin(\theta + \phi) = \sin\theta \cos\phi - \cos\theta \sin\phi \tag{B.2}$$

Small angle approximation for sine

$$\sin\delta\theta \approx \delta\theta, \qquad \delta\theta << 1 \tag{B.3}$$

Small angle approximation for cosine

$$\cos\delta\theta \approx 1, \qquad \delta\theta << 1 \tag{B.4}$$

Cramer's rule

Assuming a system of equations

$$\begin{aligned} a_1 x + b_1 y &= c_1 \\ a_2 x + b_2 y &= c_2, \end{aligned}$$

Cramer's rule yields the following solutions

$$x = \frac{c_1 b_2 - b_1 c_2}{a_1 b_2 - b_1 a_2} \tag{B.5}$$

$$y = \frac{a_1 c_2 - c_1 a_2}{a_1 b_2 - b_1 a_2} \tag{B.6}$$

B.2 Derivations

Explicit calculation of 2-box model temperature difference

Writing out and canceling terms of the polar-tropics temperature anomaly difference:

$$\begin{aligned} f(\Delta T_2 - \Delta T_1) = &- 4\epsilon\sigma T_1^3 s_2 \Delta\alpha_2 - 4\epsilon\sigma T_1^3 \Delta\epsilon T_2^4 - 4\epsilon\sigma T_1^3 n\gamma \Delta H (T_2 - T_1) \\ &- \cancel{\gamma H s_2 \Delta\alpha_2} - \cancel{\gamma H \Delta\epsilon T_2^4} - \cancel{n\gamma^2 H \Delta H (T_2 - T_1)} \\ &- \cancel{n\gamma H s_1 \Delta\alpha_1} - \cancel{n\gamma H \Delta\epsilon T_1^4} + \cancel{n\gamma^2 H \Delta H (T_2 - T_1)} \\ &+ 4\epsilon\sigma T_2^3 s_1 \Delta\alpha_1 + 4\epsilon\sigma T_2^3 \Delta\epsilon T_1^4 - 4\epsilon\sigma T_2^3 \gamma \Delta H (T_2 - T_1) \\ &+ \cancel{n\gamma H s_1 \Delta\alpha_1} + \cancel{n\gamma H \Delta\epsilon T_1^4} - \cancel{n\gamma^2 H \Delta H (T_2 - T_1)} \\ &+ \cancel{\gamma H s_2 \Delta\alpha_2} + \cancel{\gamma H \Delta\epsilon T_2^4} + \cancel{n\gamma^2 H \Delta H (T_2 - T_1)}, \end{aligned} \tag{B.7}$$

APPENDIX C

Computer Code

The following python class is an implementation of the diffusion model employing a finite difference scheme. This code was developed prior to the author having a full understanding of the analytical expressions and so notation and logical structure may be different of that presented in Section 3.

```
import sys

import numpy as np


class Diffusion: # 12.1e7
    def __init__(self, dtheta, dt=0, endtime=1.21e8, diffusivity=1e7, height=1e4, spherical=True):
        self.R = 6371e3
        self.sigma = 5.67e-8
        self.density = 1.3
        self.specific_heat = 1004

        self.dtheta = dtheta
        self.endtime = endtime
        self.spherical = spherical

        self.nboxes = round(np.pi/dtheta) + 1
        self.latitude = np.linspace(-89, 89, self.nboxes)*np.pi/180
        self.incoming = np.zeros_like(self.latitude)
        self.outgoing = np.zeros_like(self.latitude)
        self.constraint = np.zeros_like(self.latitude)

        if self.spherical:
            geometricTerm = np.tan(self.latitude)
        else:
            geometricTerm = 0

        if callable(diffusivity):
            self.diffusivity = diffusivity(self.latitude)
        else:
            self.diffusivity = np.ones_like(self.latitude)*diffusivity

        if callable(height):
            self.height = height(self.latitude)
        else:
            self.height = np.ones_like(self.latitude)*height

        if dt == 0:
            self.dt = 0.4*(self.R*self.dtheta)**2/np.max(self.diffusivity)
        else:
```

```
            self.dt = dt

        self.timepoints = round(self.endtime/self.dt) + 1
        self.s = self.diffusivity*self.dt/(self.R*self.dtheta)**2
        self.temperature = np.zeros(self.nboxes)
        self.velocity = self.diffusivity*(geometricTerm \
                                    - np.gradient(self.diffusivity, self.latitude)\
                                    /self.diffusivity \
                                    - np.gradient(self.height, self.latitude)\
                                    /self.height) \
                                    /self.R
        self.C0 = self.velocity*self.dt/(self.dtheta*self.R)

        try:
            assert(self.s[self.s >= 0.5].size == 0)
        except AssertionError:
            s = np.mean(self.s[self.s >= 0.5])
            print(f"Numerical method is unstable, {s:.2f} > 0.5 please choose another dt.")
            sys.exit(0)
        return

    def Fs(self, temperature, solarConstant, albedo, emissivity):
        self.incoming = solarConstant*(1 - albedo)
        self.outgoing = emissivity*self.sigma*temperature**4
        if self.spherical:
            self.constraint = np.sum((self.incoming - self.outgoing)*np.cos(self.latitude))
        else:
            self.constraint = np.sum(self.incoming - self.outgoing)
        self.netSolarFlux = (self.incoming - self.outgoing)/(self.density*self.specific_heat*self.heigh
        return self.netSolarFlux

    def run(self, solarConstant=350, albedo=0.3, emissivity=0.6):
        if callable(solarConstant):
            solarConstant = solarConstant(self.latitude)
        if callable(albedo):
            albedo = albedo(self.latitude)
        if callable(emissivity):
            emissivity = emissivity(self.latitude)

        self.temperature = np.zeros_like(self.temperature)
        self.incoming = np.zeros_like(self.latitude)
        self.outgoing = np.zeros_like(self.latitude)
        self.constraint = np.zeros_like(self.latitude)
        # initialise matrix elements
        c0 = (self.s + self.C0/2)
        c0[-1] = 2*self.s[-1]
        c1 = 1 - 2*self.s
        c2 = (self.s - self.C0/2)
        c2[0] = 2*self.s[0]
        dummytemp0 = np.zeros_like(self.temperature)
        dummytemp2 = np.zeros_like(self.temperature)
        for n in range(self.timepoints - 1):
            Fs = self.Fs(self.temperature, solarConstant, albedo, emissivity)
            dummytemp0[1:] = self.temperature[:-1]
            dummytemp2[:-1] = self.temperature[1:]
            self.temperature = c0*dummytemp0 \
                             + c1*self.temperature \
                             + c2*dummytemp2 \
                             + Fs*self.dt
        self.diffusion_operator = np.gradient(1.3*1004*self.diffusivity \
                                        /self.R**2*self.height*np.cos(self.latitude) \
                                        *np.gradient(self.temperature, self.latitude),\
```

```
                                        self.latitude) \
                                        /np.cos(self.latitude)
        return self.temperature

    def calculate_heat_transport(self):
        dtheta = abs(self.latitude[1] - self.latitude[0])
        if self.spherical:
            self.heat_transport = 2*np.pi*self.R**2*dtheta* \
                                  np.cumsum((self.incoming - self.outgoing) \
                                  *np.cos(self.latitude))
        else:
            self.heat_transport = 2*np.pi*self.R**2*dtheta* \
                                  np.cumsum(self.incoming - self.outgoing)
        return self.heat_transport

    def calculate_heat_flux(self):
        dtheta = abs(self.latitude[1] - self.latitude[0])
        if self.spherical:
            self.heat_flux = np.cumsum( (self.incoming - self.outgoing) \
                             *np.cos(self.latitude) )*self.R*dtheta/self.height
        else:
            self.heat_flux = np.cumsum( (self.incoming - self.outgoing) ) \
                             *self.R*dtheta/self.height
        return
```

The next python class is an implementation of the MEP model, solved using two iterations of Newton's method, first for maximizing entropy production and calculating a temperature profile, then for minimizing net energy (ensuring energy conservation).

```
import numpy as np
from scipy.optimize import newton


class AMEP:
    def __init__(self, nboxes=64, height=1e4, solarConstant=450, albedo=0.3, emissivity=0.60):
        self.sigma = 5.67e-8
        self.earth_radius = 6371e3
        self.specific_heat = 1004
        self.density = 1.3
        self.nboxes = nboxes
        self.latitude = np.linspace(-np.pi/2, np.pi/2, self.nboxes - 1)
        self.temperature = np.ones(self.nboxes - 1)*273
        self.heat_transport = None
        self.heat_flux = np.zeros(self.nboxes - 1)
        #self.height = (16e3 - 9e3)/2*np.cos(2*self.latitude) + (16e3 + 9e3)/2

        if callable(height):
            self.height = height(self.latitude)
        else:
            self.height = np.ones_like(self.latitude)*height

        if callable(solarConstant):
            self.solarConstant = solarConstant(self.latitude)
        else:
            self.solarConstant = np.ones_like(self.latitude)*solarConstant

        if callable(albedo):
            self.albedo = albedo(self.latitude)
        else:
            self.albedo = np.ones_like(self.latitude)*albedo
```

```
        if callable(emissivity):
            self.emissivity = emissivity(self.latitude)
        else:
            self.emissivity = np.ones_like(self.latitude)*emissivity
        return

    def f(self, temperature, beta):
        func = temperature**4*(4*beta*temperature + 3) \
            + self.solarConstant*(1 - self.albedo) \
            /(self.emissivity*self.sigma)
        return func

    def df(self, temperature, beta):
        func = 2*temperature**3*(10*beta*temperature + 6)
        return func

    def _tune_temperature(self, beta):
        temperature = newton(self.f, self.temperature - 3/(4*beta), args=(beta, ), fprime=self.df)
        return temperature

    def _calculate_constraint(self, beta):
        temperature = self._tune_temperature(beta)
        self.incoming = self.solarConstant*(1 - self.albedo)
        self.outgoing = self.emissivity*self.sigma*temperature**4
        constraint = np.sum((self.outgoing - self.incoming)*np.cos(self.latitude))
        return constraint

    def tune_beta(self, *args, show_constraint=False, **kwargs):
        self.temperature = np.ones(self.nboxes - 1)*273
        beta = newton(self._calculate_constraint, *args, **kwargs)
        if show_constraint:
            print(self._calculate_constraint(beta))
        return beta

    def compute_temperature(self, beta):
        self.temperature = self._tune_temperature(beta)
        self._calculate_heat_transport()
        self._calculate_heat_flux()
        return self.temperature

    def _calculate_heat_transport(self):
        dtheta = abs(self.latitude[1] - self.latitude[0])
        self.heat_transport = 2*np.pi*self.earth_radius**2*dtheta* \
                              np.cumsum((self.incoming - self.outgoing) \
                              *np.cos(self.latitude))
        return

    def _calculate_heat_flux(self):
        dtheta = abs(self.latitude[1] - self.latitude[0])
        self.heat_flux = np.cumsum( (self.solarConstant*(1 - self.albedo) \
                         - self.emissivity*self.sigma*self.temperature**4) \
                         *np.cos(self.latitude) )*self.earth_radius*dtheta/self.height
        return
```

Bibliography

Armour, K. C., Siler, N., Donohoe, A. and Roe, G. H. (2019). 'Meridional atmospheric heat transport constrained by energetics and mediated by large-scale diffusion'. In: *Journal of Climate* vol. 32, no. 12, pp. 3655–3680.

Bekryaev, R. V., Polyakov, I. V. and Alexeev, V. A. (2010). 'Role of polar amplification in long-term surface air temperature variations and modern Arctic warming'. In: *Journal of Climate* vol. 23, no. 14, pp. 3888–3906.

Budyko, M. I. (1969). 'The effect of solar radiation variations on the climate of the Earth'. In: *tellus* vol. 21, no. 5, pp. 611–619.

Dai, A., Luo, D., Song, M. and Liu, J. (2019). 'Arctic amplification is caused by sea-ice loss under increasing CO 2'. In: *Nature communications* vol. 10, no. 1, pp. 1–13.

Donohoe, A., Armour, K. C., Roe, G. H., Battisti, D. S. and Hahn, L. (2020). 'The partitioning of meridional heat transport from the Last Glacial Maximum to CO2 quadrupling in coupled climate models'. In: *Journal of Climate* vol. 33, no. 10, pp. 4141–4165.

Donohoe, A. and Battisti, D. S. (2011). 'Atmospheric and surface contributions to planetary albedo'. In: *Journal of Climate* vol. 24, no. 16, pp. 4402–4418.

Gitelman, A. I., Risbey, J. S., Kass, R. E. and Rosen, R. D. (1997). 'Trends in the surface meridional temperature gradient'. In: *Geophysical research letters* vol. 24, no. 10, pp. 1243–1246.

Gjermundsen, A., LaCasce, J. H. and Graff, L. S. (May 2014). 'The Atmospheric Response to Surface Heating under Maximum Entropy Production'. In: *Journal of the Atmospheric Sciences* vol. 71, no. 6, pp. 2204–2220. eprint: https://journals.ametsoc.org/jas/article-pdf/71/6/2204/3821899/jas-d-13-0181_1.pdf.

Hahn, L., Armour, K., Battisti, D., Pauling, A., Donohoe, A. and Bitz, C. M. (2019). 'Understanding Asymmetries in Arctic and Antarctic Lapse-Rate Feedbacks and Polar Amplification'. In: *AGU Fall Meeting Abstracts*. Vol. 2019, A52A–03.

Hahn, L. C., Armour, K. C., Battisti, D. S., Donohoe, A., Pauling, A. and Bitz, C. (2020). 'Antarctic elevation drives hemispheric asymmetry in polar lapse rate climatology and feedback'. In: *Geophysical Research Letters* vol. 47, no. 16, e2020GL088965.

Hardiman, S. C., Andrews, M. B., Andrews, T., Bushell, A. C., Dunstone, N. J., Dyson, H., Jones, G. S., Knight, J. R., Neininger, E., O'Connor, F. M. et al. (2019). 'The impact of prescribed ozone in climate projections run with

HadGEM3-GC3. 1'. In: *Journal of Advances in Modeling Earth Systems* vol. 11, no. 11, pp. 3443–3453.

Hartmann, D. L. (2015). *Global physical climatology*. Vol. 103. Newnes.

Hu, S. and Vallis, G. K. (2019). 'Meridional structure and future changes of tropopause height and temperature'. In: *Quarterly Journal of the Royal Meteorological Society* vol. 145, no. 723, pp. 2698–2717.

LaCasce, J. H. (2020). 'Physical Processes in the Geosciences'.

Lindstrøm, T. and Hveberg, K. (2015). *Flervariabel analyse med lineær algebra*. Gyldendal akademisk.

Mahlstein, I. and Knutti, R. (2011). 'Ocean heat transport as a cause for model uncertainty in projected Arctic warming'. In: *Journal of Climate* vol. 24, no. 5, pp. 1451–1460.

Marshall, J., Scott, J. R., Armour, K. C., Campin, J.-M., Kelley, M. and Romanou, A. (2015). 'The ocean's role in the transient response of climate to abrupt greenhouse gas forcing'. In: *Climate Dynamics* vol. 44, no. 7-8, pp. 2287–2299.

North, G. R. (1975). 'Theory of energy-balance climate models'. In: *Journal of Atmospheric Sciences* vol. 32, no. 11, pp. 2033–2043.

O'brien, D. and Stephens, G. (1995). 'Entropy and climate. II: Simple models'. In: *Quarterly Journal of the Royal Meteorological Society* vol. 121, no. 527, pp. 1773–1796.

Overland, J., Dunlea, E., Box, J. E., Corell, R., Forsius, M., Kattsov, V., Olsen, M. S., Pawlak, J., Reiersen, L.-O. and Wang, M. (2019). 'The urgency of Arctic change'. In: *Polar Science* vol. 21, pp. 6–13.

Ozawa, H., Ohmura, A., Lorenz, R. D. and Pujol, T. (2003). 'The second law of thermodynamics and the global climate system: A review of the maximum entropy production principle'. In: *Reviews of Geophysics* vol. 41, no. 4.

Paltridge, G. W. (1975). 'Global dynamics and climate-a system of minimum entropy exchange'. In: *Quarterly Journal of the Royal Meteorological Society* vol. 101, no. 429, pp. 475–484.

Pistone, K., Eisenman, I. and Ramanathan, V. (2014). 'Observational determination of albedo decrease caused by vanishing Arctic sea ice'. In: *Proceedings of the National Academy of Sciences* vol. 111, no. 9, pp. 3322–3326.

Pujol, T. and Fort, J. (2002). 'States of maximum entropy production in a onedimensional vertical model with convective adjustment'. In: *Tellus A: Dynamic Meteorology and Oceanography* vol. 54, no. 4, pp. 363–369.

Santer, B. D., Wehner, M. F., Wigley, T., Sausen, R., Meehl, G., Taylor, K., Ammann, C., Arblaster, J., Washington, W., Boyle, J. et al. (2003). 'Contributions of anthropogenic and natural forcing to recent tropopause height changes'. In: *science* vol. 301, no. 5632, pp. 479–483.

Schaefer, K., Lantuit, H., Romanovsky, V. E., Schuur, E. A. and Witt, R. (2014). 'The impact of the permafrost carbon feedback on global climate'. In: *Environmental Research Letters* vol. 9, no. 8, p. 085003.

Screen, J. A. and Simmonds, I. (2010). 'The central role of diminishing sea ice in recent Arctic temperature amplification'. In: *Nature* vol. 464, no. 7293, pp. 1334–1337.

Sellers, W. D. (1969). 'A global climatic model based on the energy balance of the earth-atmosphere system'. In: *Journal of Applied Meteorology and Climatology* vol. 8, no. 3, pp. 392–400.

Smith, D. M., Screen, J. A., Deser, C., Cohen, J., Fyfe, J. C., Garcıa-Serrano, J., Jung, T., Kattsov, V., Matei, D., Msadek, R. et al. (2019). 'The Polar Amplification Model Intercomparison Project (PAMIP) contribution to CMIP6: Investigating the causes and consequences of polar amplification'. In: *Geoscientific Model Development* vol. 12, no. 3, pp. 1139–1164.

Stephens, G. and O'brien, D. (1993). 'Entropy and climate. I: ERBE observations of the entropy production of the earth'. In: *Quarterly Journal of the Royal Meteorological Society* vol. 119, no. 509, pp. 121–152.

Stone, P. H. (1978). 'Constraints on dynamical transports of energy on a spherical planet'. In: *Dynamics of atmospheres and oceans* vol. 2, no. 2, pp. 123–139.

Stuecker, M. F., Bitz, C. M., Armour, K. C., Proistosescu, C., Kang, S. M., Xie, S.-P., Kim, D., McGregor, S., Zhang, W., Zhao, S. et al. (2018). 'Polar amplification dominated by local forcing and feedbacks'. In: *Nature Climate Change* vol. 8, no. 12, pp. 1076–1081.

Thiebaux, M. (1976). 'One-particle, two-dimensional effective eddy diffusivities from balloon trajectories'. In: *Journal of Atmospheric Sciences* vol. 33, no. 6, pp. 1050–1059.

Vallis, G. K., Zurita-Gotor, P., Cairns, C. and Kidston, J. (2015). 'Response of the large-scale structure of the atmosphere to global warming'. In: *Quarterly Journal of the Royal Meteorological Society* vol. 141, no. 690, pp. 1479–1501.